Title

Circularly Polarized Low Side Lobe Level Composite Right/Left-Handed SIW Leaky Wave Antenna and Blazed Metasurface

Author

Li, Xiaoqiang

Publication Date

2016

Peer reviewed|Thesis/dissertation

UNITVERSITY OF CALIFORNIA

Los Angeles

Circularly Polarized Low Side Lobe Level Composite Right/Left-Handed SIW Leaky Wave Antenna and Blazed Metasurface

A thesis submitted in partial satisfaction

of the requirements for the degree

Master of Science in Electrical Engineering

by

Xiaoqiang Li

2016

ABSTRACT OF THE THESIS

Circularly Polarized Low Side Lobe Level Composite Right/Left Handed SIW Leaky Wave Antenna and Blazed Metasurface

by

Xiaoqiang Li

Master of Science in Electrical Engineering Department

University of California, Los Angeles, 2016

Professor Tatsuo Itoh, Chair

A brief review of composite right/left handed (CRLH) transmission line (TL) theory and CRLH substrate integrated waveguide (SIW) leaky wave antennas (LWAs) is presented. Further, a work of circularly polarization (CP) low side lobe level (SLL) CRLH SIW LWA is shown. The SLL reduction is achieved by tapering the radiation amount in each radiation unit along the LWA. In the second part, the principle of diffraction gratings are summarized. In addition, a set of novel planar metasurface structures are proposed to behave as a 3D diffraction grating such that the specular reflection is minimized. The feature is obtained by utilizing both periodicity of the super unit structure and phase modulation provided in the unit cells. Two different designs of such structure are given following the same methodology. The metasurface then is applied to a rectangular waveguide to create a stopband structure.

The thesis of Xiaoqiang Li is approved.

Benjamin S. Williams

Yuanxun Wang

Tatsuo Itoh, Committee Chair

University of California, Los Angeles

2016

To my beloved families.

TABLE OF CONTENTS

TABLE OF FIGURES

TABLE OF TABLES

ACKNOWLEDGEMENT

First, I would like to express my sincere gratitude to Professor Tatsuo Itoh for his guidance for my master's study. It was him who gave me the chance to do research and showed me how to be a good researcher.

I would like to thank Doctor Mohammad Memarian for his direct guidance in my project. His knowledge and experiences greatly helped me in the project.

I would also like to thank Amogh Waghmare, Hanseung Lee, Kirti Dwaj, Yasuo Morimoto, Zhi Shen. They warmly welcome me to the lab and gave me a lot of help. I feel so lucky to be able to work with them in the same lab.

I would like to thank all the friends here in UCLA. Their company made my life colorful.

In the end, I would like to greatly thank my family. Nothing would happen without their unconditional support for me.

Chapter 1

Circularly Polarized Low Side Lobe Level Composite Right/Left Handed SIW Leaky Wave Antenna

1.1 Introduction

Composite right/left handed (CRLH) transmission line (TL) can enable leaky wave antennas (LWAs) with full-scanning capability including backward and broadside directions [1]. Nowadays the study covers not only the microwave regime but also the Terahertz range [2]. In microwave/RF frequency range, guiding structures of CRLH LWAs are typically realized by using a microstrip line or a substrate integrated waveguide (SIW) [3][4]. However a CRLH SIW LWA can be more advantageous than a microstrip based CRLH LWA because of its high power-handling capability and pure polarization characteristic. Based on a CRLH SIW technique, there have been studies to improve side lobe level (SLL) of LWAs [5]. In this chapter, approaches to improve SLL of CRLH SIW LWAs are provided based on the concept of a CRLH SIW.

1.1.1 CRLH Transmission Line

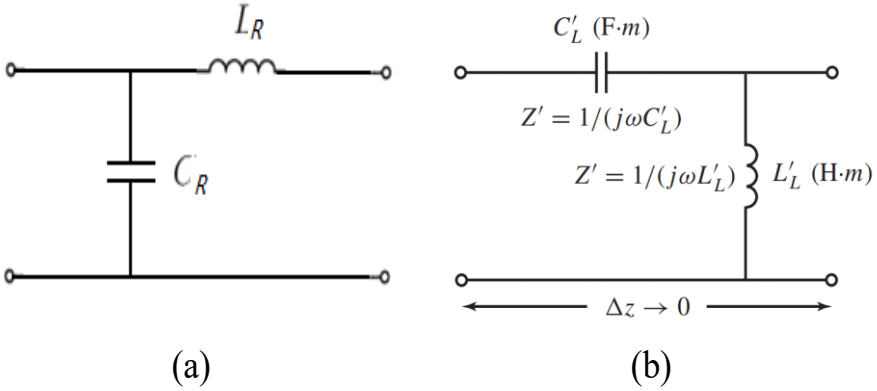

Figure 1 Increments circuit model for a hypothetical uniform TL .(a) RH TL(b) LH TL

Transmission line theory in many ways bridges the gap between field analysis and basic circuit theory [6]. The incremental circuit model of conventional transmission line is right-handed (RH) series-L/shunt-C TL and shown in Figure 1 (a). On the other hand, left-handed (LH) TL's incremental circuit model is the dual of RH TL which is shown in Figure 1(b). The principle characteristics can be easily obtained through Kirchhoff's laws. For simplicity, the lossless case is considered. Thus the complex propagation constant γ, the propagation constant β, the characteristic impedance Z_c, the phase velocity v_p, the group velocity v_g are given by [7]:

$$\gamma = j\beta = \sqrt{Z'Y'} = \frac{1}{j\omega\sqrt{L'_L C'_L}} = -\frac{j}{\omega\sqrt{L'_L C'_L}} \quad (1.1a)$$

$$\beta = -\frac{j}{\omega\sqrt{L'_L C'_L}} < 0 \quad (1.1b)$$

$$Zc = \sqrt{\frac{Z'}{Y'}} = \frac{L'_L}{C'_L} > 0 \quad (1.1c)$$

$$v_p = \frac{\omega}{\beta} = -\omega^2\sqrt{L'_L C'_L} < 0 \quad (1.1\ d)$$

$$v_g = (\frac{\partial\beta}{\partial\omega})^{-1} = +\omega^2\sqrt{L'_L C'_L} > 0 \quad (1.1\ e)$$

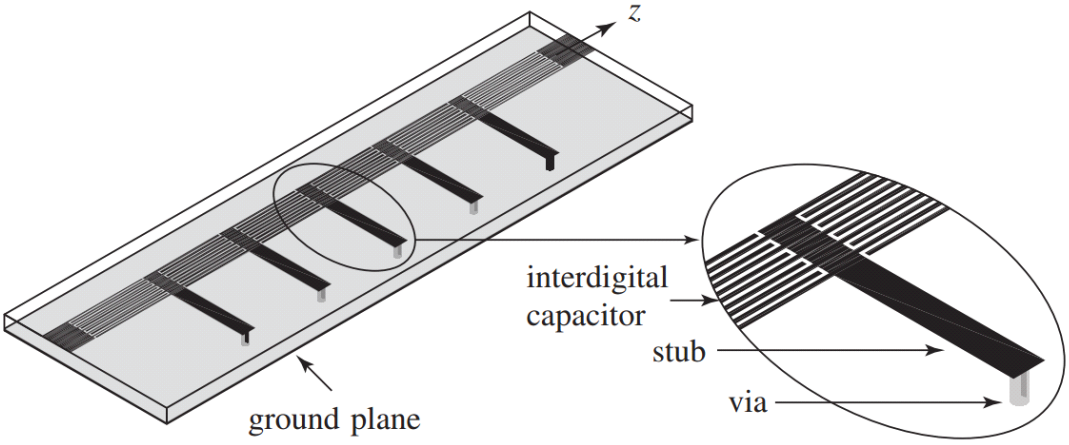

Figure 2 Microstrip CRLH transmission line

It is immediately evident that the phase velocity and group velocity have opposite signs. That means the direction of wave vector β and the direction of power propagation are

opposite in the left handed regime only. Meanwhile, it has to be kept in mind that the length of unit cell Δz has to be much smaller

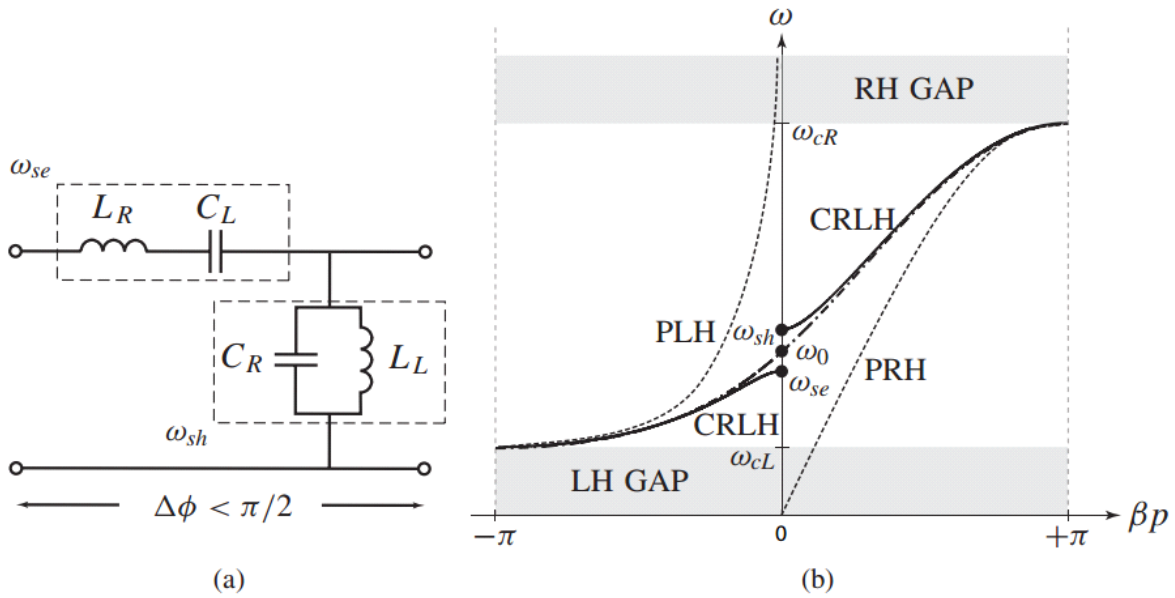

Figure 3 (a) Circuit model of CRLH TL unit cell. (b) Dispersion diagram for the pure LH (PLH), pure RH (PRH) and CRLH structure.

than the guided wavelength λ_g such that the TL can be treated as a uniform media [7]. One realization of the LH TL is implemented by microtrip technology (Figure 2) [8]. The series capacitance is given by the interdigital slots while the shunt inductance is provided by shorted stub. Nevertheless, since there is current flowing along the signal line and electric field between signal line and ground, it is inevitable to have series-L and shunt-C which contribute to RH TL. Thus, a pure LH TL cannot exist since there is always L_R and C_R in addition to L_L and C_L. In consequence, the term composite right/left-handed (CRLH) was introduced [7]. The equivalent circuit model for CRLH TL is given in Figure 3(a). At lower frequencies, L_R is nearly short and C_R is nearly open. In this scenario, the LH structure dominates. Since LH structure has high-pass nature, there is a LH bandgap below certain cutoff frequency. At higher frequencies, L_L is almost open and C_L is almost short. Thus RH structure dominates. On the

contrary, RH structure has low pass nature such that a RH band gap occurs beyond certain cut off frequency. Generally, the series resonance frequency ω_{se} and shunt resonance frequency ω_{sh} are not same which results in a bandgap between the LH range and RH range. However, if the parameters are designed such that $\omega_{se} = \omega_{sh}$, the gap disappears which allows power to transfer at $\beta = 0$ [7]. Such structure is called balanced CRLH TL and it is necessary condition if a broadside radiation pattern is desired from LWAs.

1.1.2 Leaky Wave Antennas

A leaky wave antenna is one kind of travelling wave antenna. The wave radiates while it propagates along the waveguiding structure. For instance, a slotted waveguide can be a LWA. Figure 4 shows a typical leaky wave structure. The normalized wave leaking from the structure is presented as:

$$\psi = e^{-\gamma z} e^{-k_y y} = e^{-\alpha z} e^{-\beta_z z} e^{-i k_y y} \qquad (1.2)$$

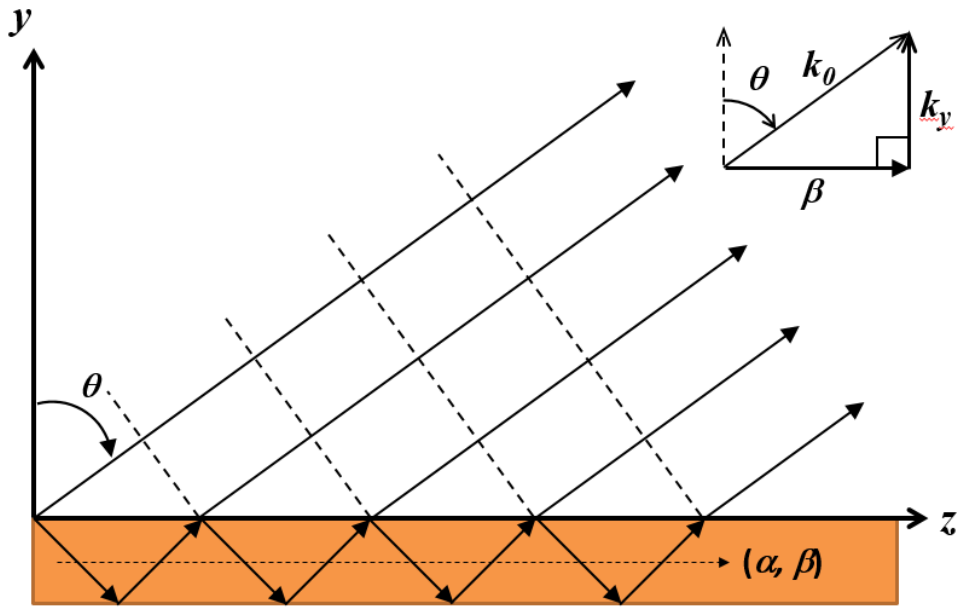

Figure 4 Schematic of a LWA and its leaky-wave operation

The propagation constant γ is complex (real part α and imaginary part β_z). α represents the decay along z direction due to losses and leakage. β_z is the wave vector. Since in free space, the leaked wave has light velocity c and wave number k_0 along the main beam direction, the propagation constant in y-direction is

$$k_y = \sqrt{k_0^2 - \beta_z^2} \qquad (1.3)$$

Note that if k_y is real or $\beta < k_0$ (fast wave), leakage radiation is occurs from the guiding structure. However, if $\beta > k_0$ (slow wave), k_y will be imaginary. Thus $e^{-ik_y y}$ term will exponentially decay along the *y*-direction. Then traveling wave inside the structure is totally guided and there is no leakage radiation. In the fast wave case, due to the phase matching at the interface, beam scanning angle θ can be controlled by β [9].

$$sin\theta = \beta/k_0 \qquad (1.4)$$

1.1.3 SIW CRLH Leaky Wave Antenna

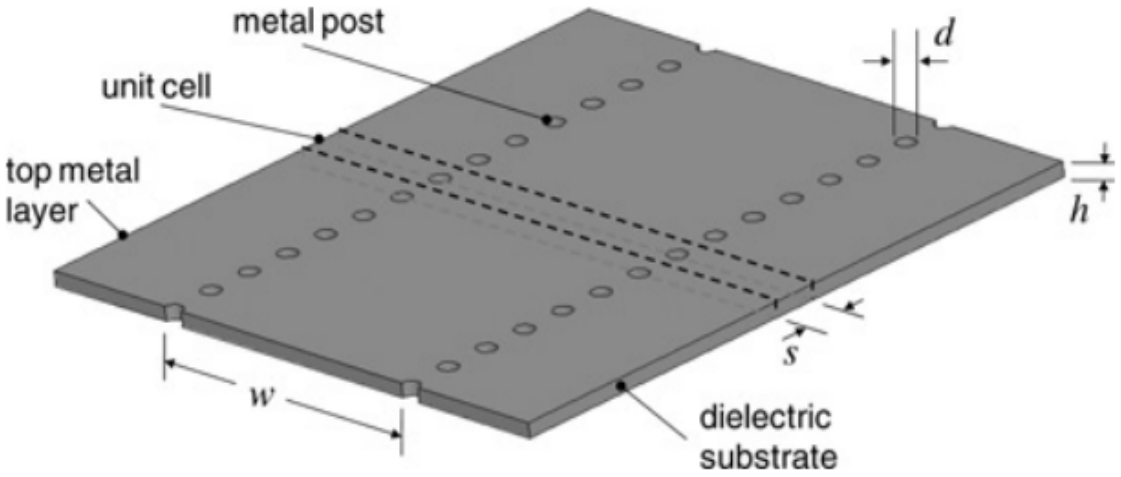

Figure 5 the geometry of SIW

Figure 5 shows the geometry of a Substrate integrate waveguide (SIW) structure. SIW is a technology to implement waveguide with a printed circuit board (PCB) process by

periodically putting vias which act as PEC walls. Together with the top and bottom layers, a rectangular waveguide is obtained. SIW has similar field distribution and dispersion diagram as a rectangular waveguide. In addition, its high Q, high power-handling capability while

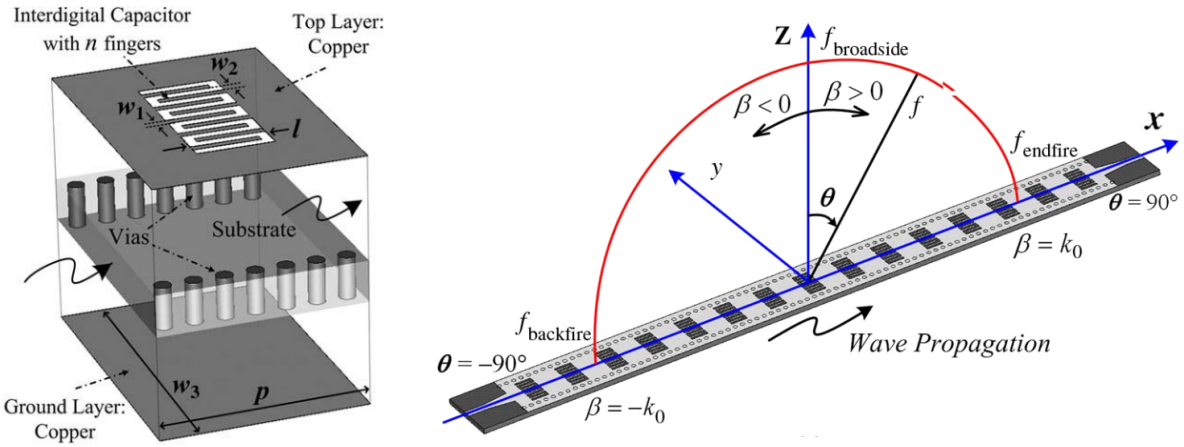

(a) (b)

Figure 6 (a) Unit cell of SIW CRLH LWA (b) Overall SIW leaky-wave antenna prototype.

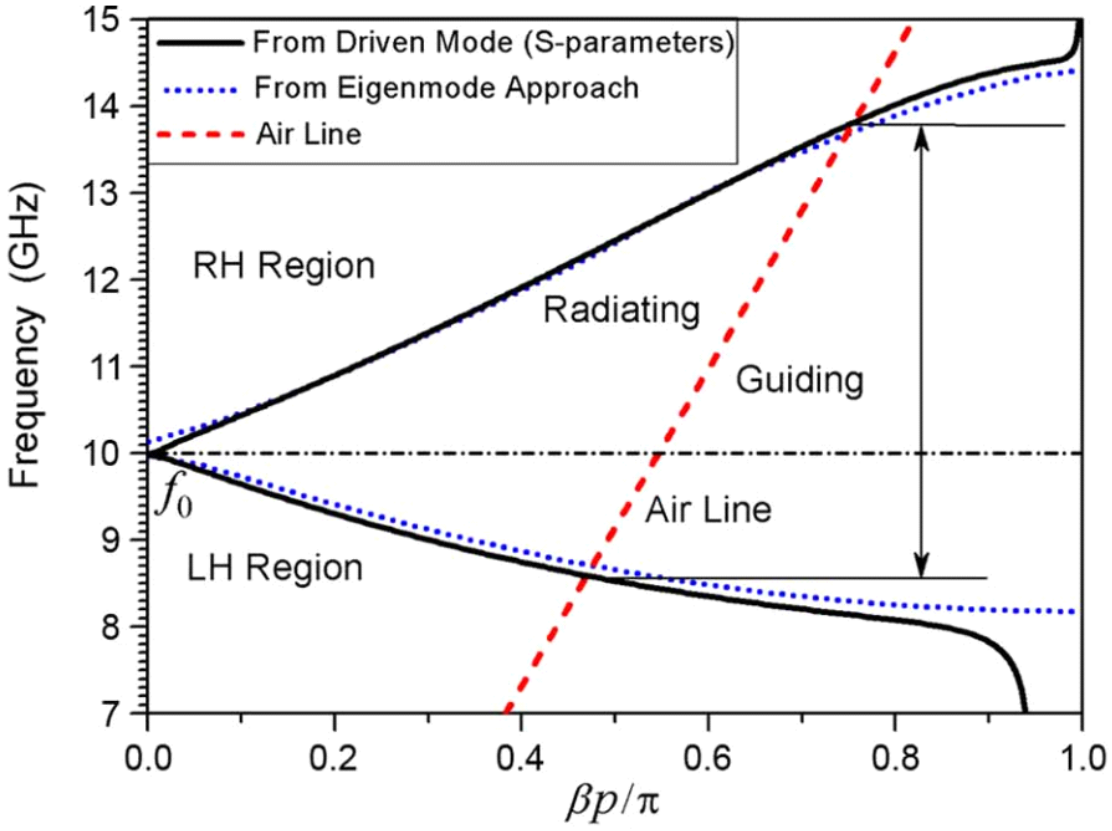

Figure 7 the dispersion diagram of the SIW CRLH LWA

maintaining a very low profile make it more preferable over waveguides in many applications [10].

Using SIW technology, a CRLH LWA is designed (Figure 6). The series capacitance is given by the interdigital slot while the shunt inductance is provided by the vias. The parameters are carefully chosen such that the SIW CRLH LWA is balanced at 10 GHz (Figure 7).

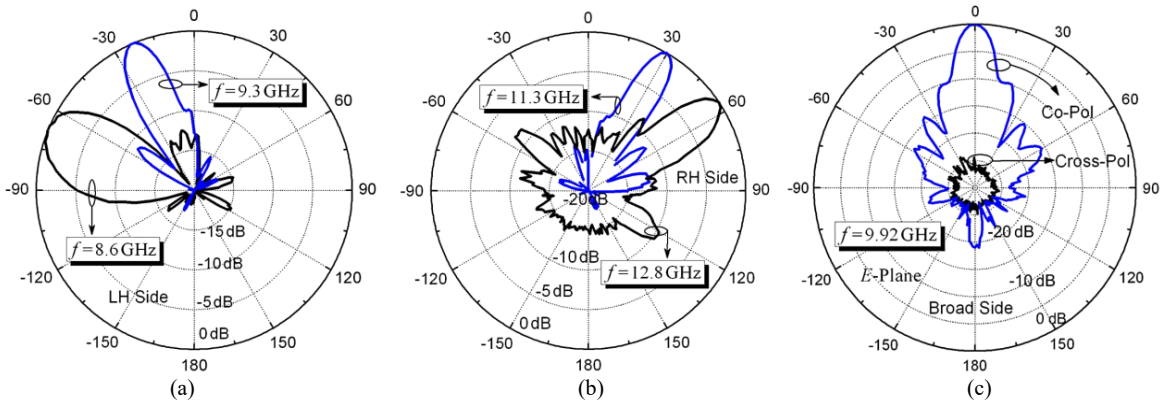

Figure 8 Measured radiation pattern (E plane). (a) LH region. (b) RH region. (c) Broad side

From the dispersion diagram, it can be expected that the proposed SIW CRLH LWA is capable of full space beam scanning. More specifically, main beam points in the forward direction for frequencies larger than 10GHz, while the main beam points in the backward direction for frequencies lower than 10GHz, and broadside radiation at 10 GHz. The measurement result confirms these expected behaviors (Figure 8) [11].

1.2 Design Guideline

In this work, all the designs are based on Rogers RT/duroid® 6010 Laminates substrate with dielectric constant of 10.2, a tangent loss of 0.0023 and a thickness of 1.27mm. The vias to build SIW has a diameter of 0.8mm and a periodicity of 1.2mm.

1.2.1 Implementation of Circularly Polarization (CP)

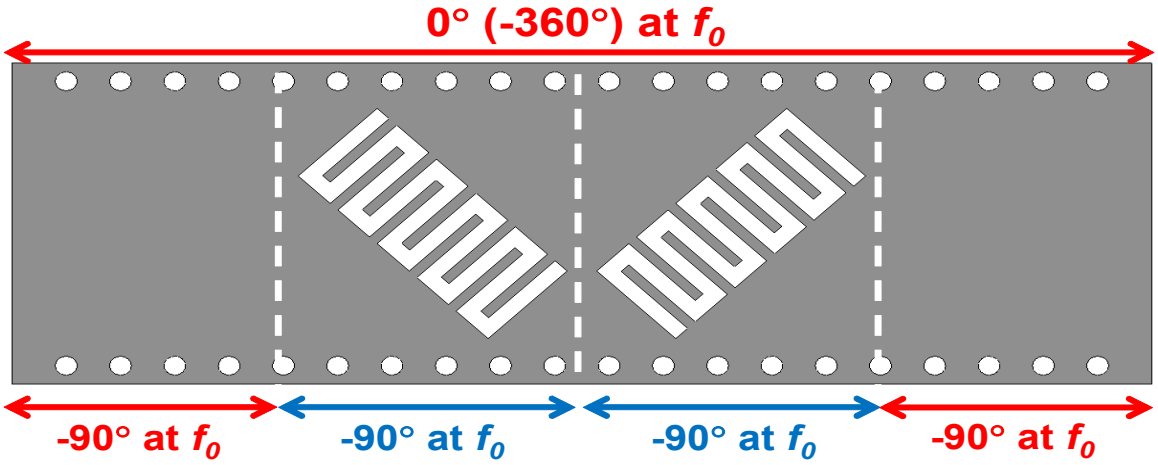

Figure 9 the unit cell of the CP SIW CRLH LWA

As shown in Figure 9[12], CP is achieved by a pair of orthogonal interdigital slots with a 90° phase delay in each unit cell. Two margin sections will provide an additional -90° phase delay each such that the total phase delay of the whole unit cell is 360°. The existence of the margin sections are important, otherwise every neighboring pair will

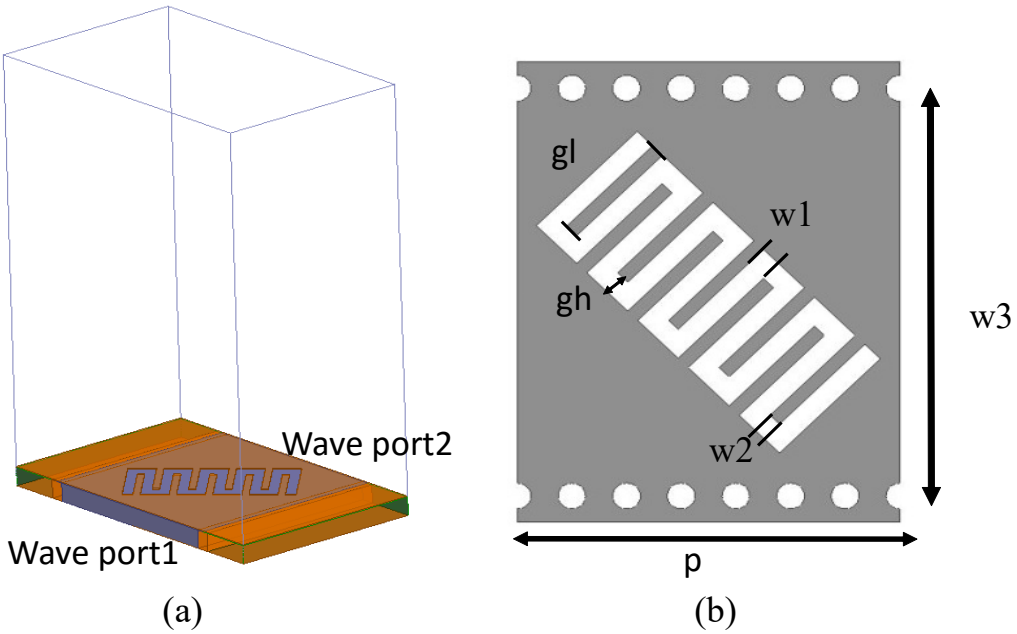

Figure 10 (a) Unit section simulation model in HFSS. (b) Details and parameters for unit section

produce an opposite CP wave which will result in cancelation with each other. To get the phase delay of the each section, a single section simulation in HFSS is required (Figure 10).

The simulation can provide the S matrix of the section and can be transferred into ABCD matrix by [6]:

$$A = \frac{(1+S_{11})(1-S_{22})+S_{12}S_{21}}{2S_{21}} \qquad (1.5)$$

By considering the structure to be a uniform TL, and for a TL having:

$$A = \cos(\beta d) \qquad (1.6)$$

The phase delay can be easily obtained by:

$$\Delta\phi = \beta d = re(\cos^{-1}(A)) \qquad (1.7)$$

Given the width of the SIW structure and the center frequency, the length of the margin sections is found for providing the 90° phase delay. However, it is difficult to design the two center sections with orthogonal interdigital slots. The reason is that the topology of the interdigital slots will intensively affect the series capacitance as well as other parameters.

1.2.2 Low Side Lobe Level

It is well known that side lobe level of antennas can be improved by tapering the radiation aperture [5]. In the LWA scenario, the leakage amount of each unit cell can be controlled so that a tapering effect is obtained. It is natural to consider controlling the leakage amount by modifying the shape of the interdigital slot. However, as previously noted, it is not straightforward to handle such a subtle structure while maintaining the 90° phase delay. In this work, we set w_2=0.4mm, w_3=12.2mm, p=12mm, g_l=3.5mm. These numbers are obtained by optimization to maintain a center frequency at 4.5GHz, and w_1 and g_h are tuned to achieve the goal.

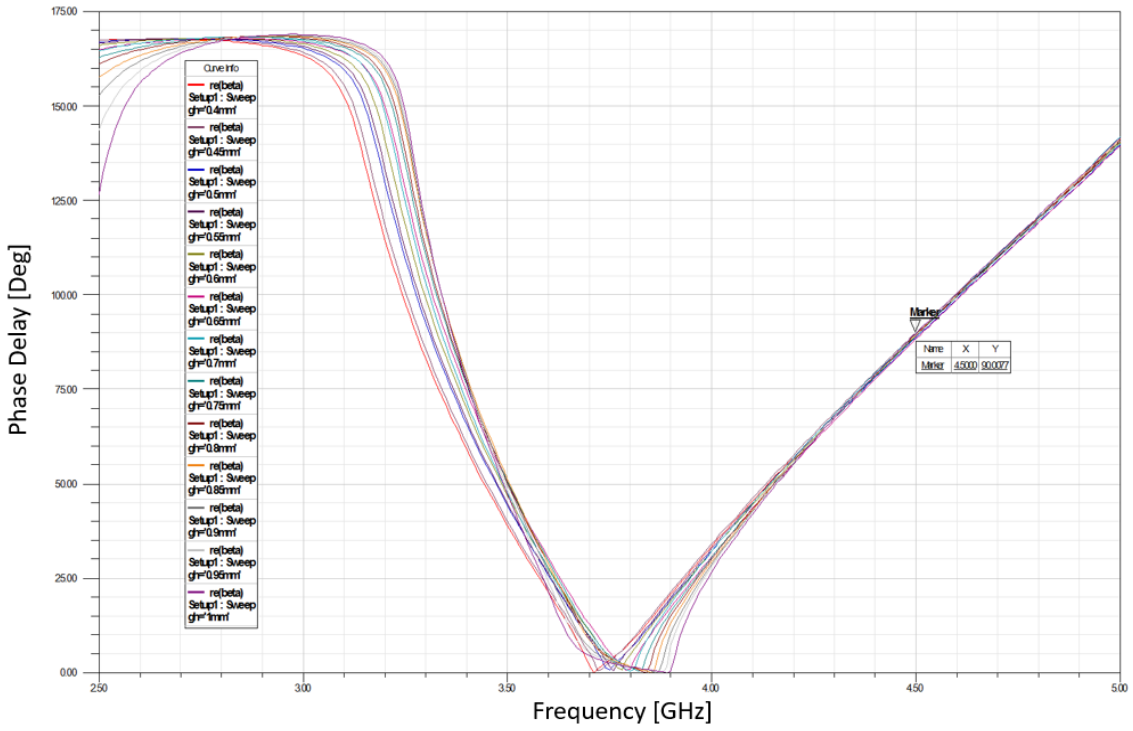

Figure 11 the dispersion diagram for the parametric sweep

One important discovery of this pair of parameters is that they are linear within a large range. The relationship is given by:

$$w_1 = 1.1 - 0.5g_h \qquad (1.8)$$

To verify the equation, a parametric sweep in simulation is performed. In simulation, g_h is swept from 0.45mm to 1mm. On the other hand, w_1 is accommodated with the g_h by using equation (1.8). The dispersion diagram is obtained (Figure 11). From the dispersion diagram, we can easily find that at 4.5 GHz, the phase delay is perfectly maintained at 90°. This results in an effective method for manipulating the interdigital slots. A further investigation is needed to research the leakage amount of the section with different interdigital slots. To get the leakage amount, a similar simulation as shown in Figure 10(a) is required. However, in this measurement, all materials are set to be lossless. In this case, all power dissipation is only caused by to the leakage, and that the leakage amount can be characterized as:

$$Leakage = 1 - |S11|^2 - |S21|^2 \qquad (1.9)$$

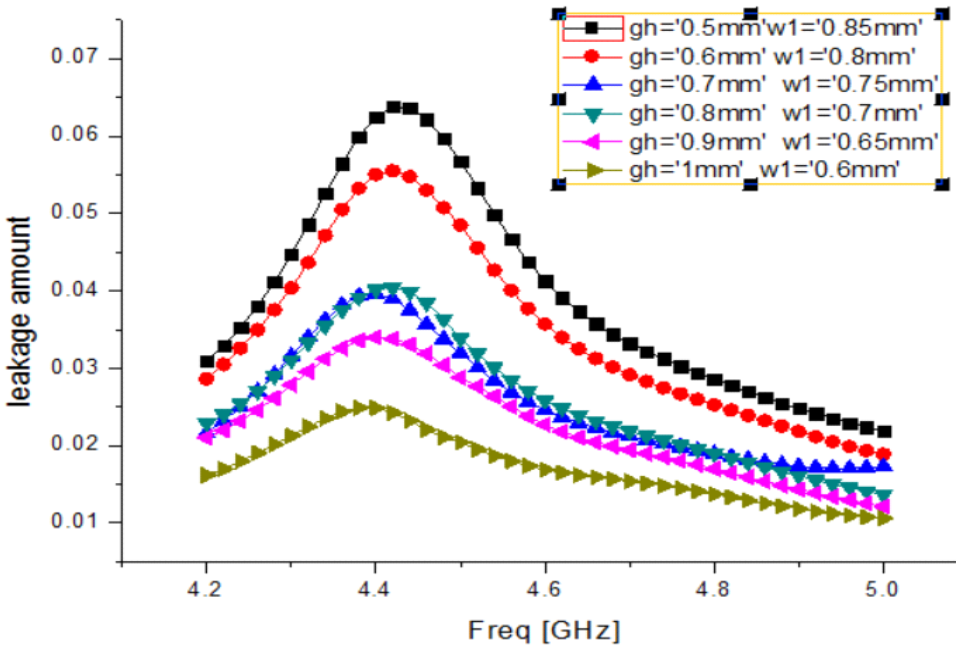

Figure 12 Leakage amount for different pairs of g_h and w_1. p=12mm, w_2=0.4mm,w_3=12.2mm.g_l=3.5

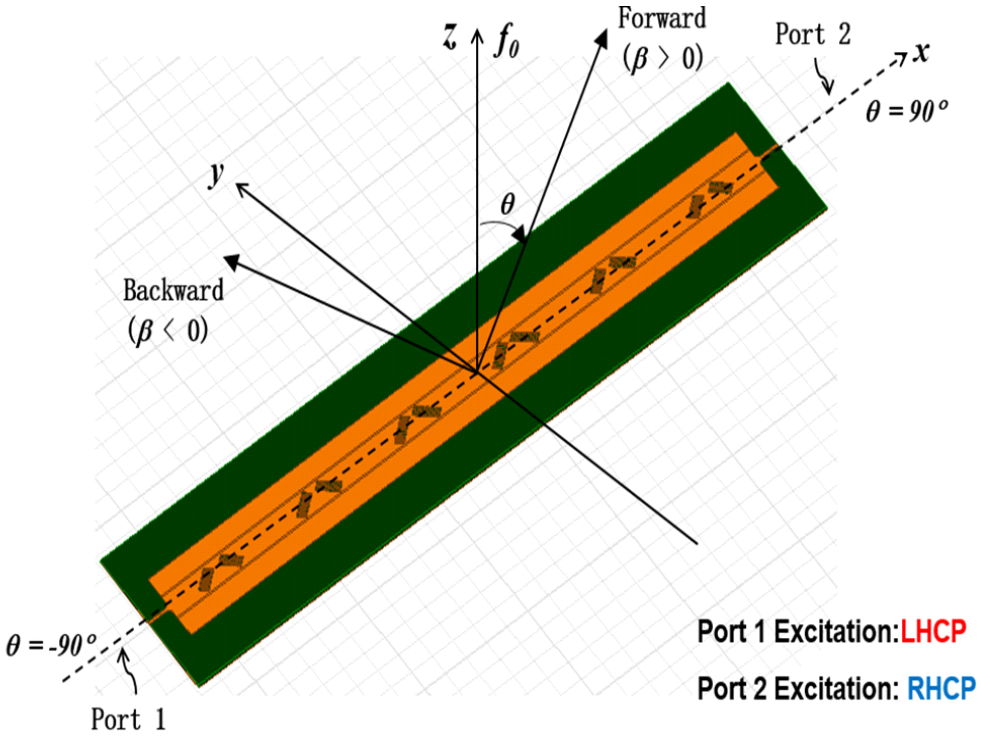

Figure 13 the topology of the proposed leaky wave antenna

A few pairs of parameters are selected to calculate the leakage amount (Figure 12). It can be seen from the graph that the highest leakage amount can be three times as high as the lowest case. The control over leakage amount per section can therefore be implemented.

1.2.3 The Layout of the Antenna

A six cell prototype is designed to demonstrate the low side lobe level effect (Figure 13). The substrate and other parameters are mentioned before. While for different unit cells, the w_1 and g_h combinations are different. The two unit cells in the center have the pair which corresponds to the largest leakage amount; the two unit cells in the ends have the smallest leakage amount; the remaining two cells between center and end units have the medium leakage amount. For simplicity, the leakage amount is linearly tapered. The combinations are shown in Table 1.

Table 1 designing parameter pairs

Unit Cell Position	g_h/mm	w_1/mm	Leakage
Center	0.6	0.8	0.055
Middle	0.8	0.7	0.040
End	1	0.6	0.025

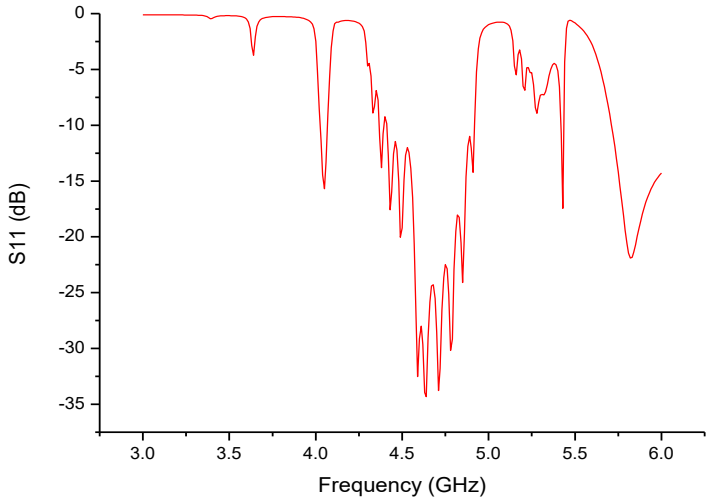

Figure 14 S_{11} of the proposed antenna with tapered feeding line

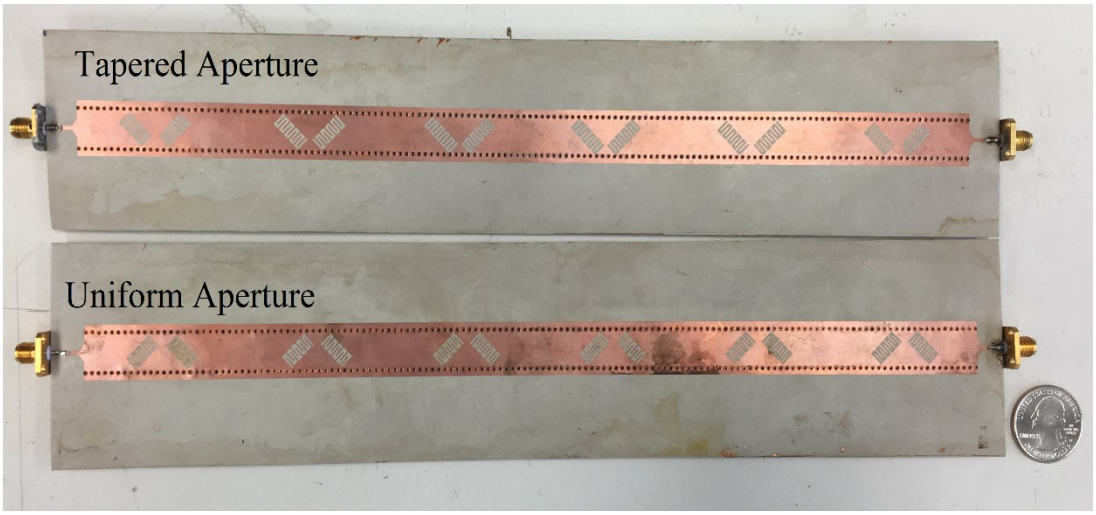

Figure 15 the fabricated leaky wave antennas

The feeding lines are 50Ω microstrip lines tapered in the end to match the impedance. Simulation shows that a passband from 4.4 GHz to 4.9 GHz (Figure 14). It has to be noticed that matching the impedance near 4.5 GHz is difficult because this LWA is a periodic structure

and that 4.5 GHz is at the edge of its Brillouin zone. That makes 4.5 GHz naturally in the bandgap. However, the cells number is not too large which makes it still possible to be matched.

1.3 Measurement of the Proposed Leaky Wave Antenna

In order to compare the proposed low side lobe antenna with the conventional antenna, two antennas are fabricated and measured (Figure 15). The first one is the tapered leakage amount case which is mentioned in last section. The other one is the same structure except that the interdigital slots are uniform in all unit cells. In this uniform antenna, g_h = 0.6mm, w_1=0.8mm, which is the case for the middle unit cells in the tapered antenna. The measurements are

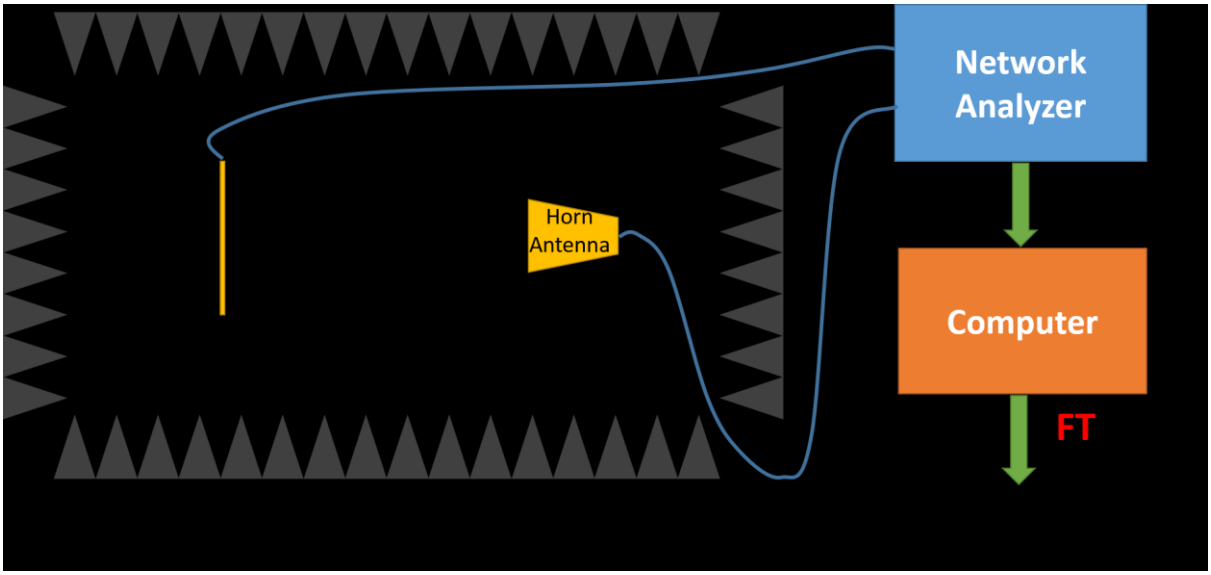

Figure 16 Measurement setup

performed over three frequency, 4.5 GHz, 4.6 GHz and 4.7GHz. The radiation pattern and circularly polarization are measured both for the uniform and tapered antennas.

1.3.1 Measurement Setup

The measurements are performed in UCLA center for high frequency electronics (CHFE) near field chamber. The near field measurement is performed and the results are transferred

into far field using Fourier transform. Considering that leaky wave antenna is a two port device, one port is connected to the network analyzer and the other port is terminated with $50\ \Omega$ load. The measurement set up is shown in Figure 16.

1.3.2 Radiation Pattern Measurements

The normalized gain of both conventional and tapered LWA in x-z plane are presented in Figure 17. It can be seen that the side lobe level of the tapered LWA is generally 3 dB lower compared with the conventional ones in all cases. This shows that the tapering of the leakage amount indeed reduces the side lobe level. Another observation is that near broadside radiation is achieved near 4.5 GHz. The main beam is between 1.8 to -12°. The broad side indicates that a $\pi/2$ phase delay happens over each unit section at that frequency thus a 2π phase delay is obtained over the whole unit cell. The small shift of the center frequency is due to fabrication error. Meanwhile, the main beam is between -1.2 to 13.2° at 4.6 GHz and 8 to 22.2° at 4.7GHz.

1.3.3 Circularly Polarization Measurements

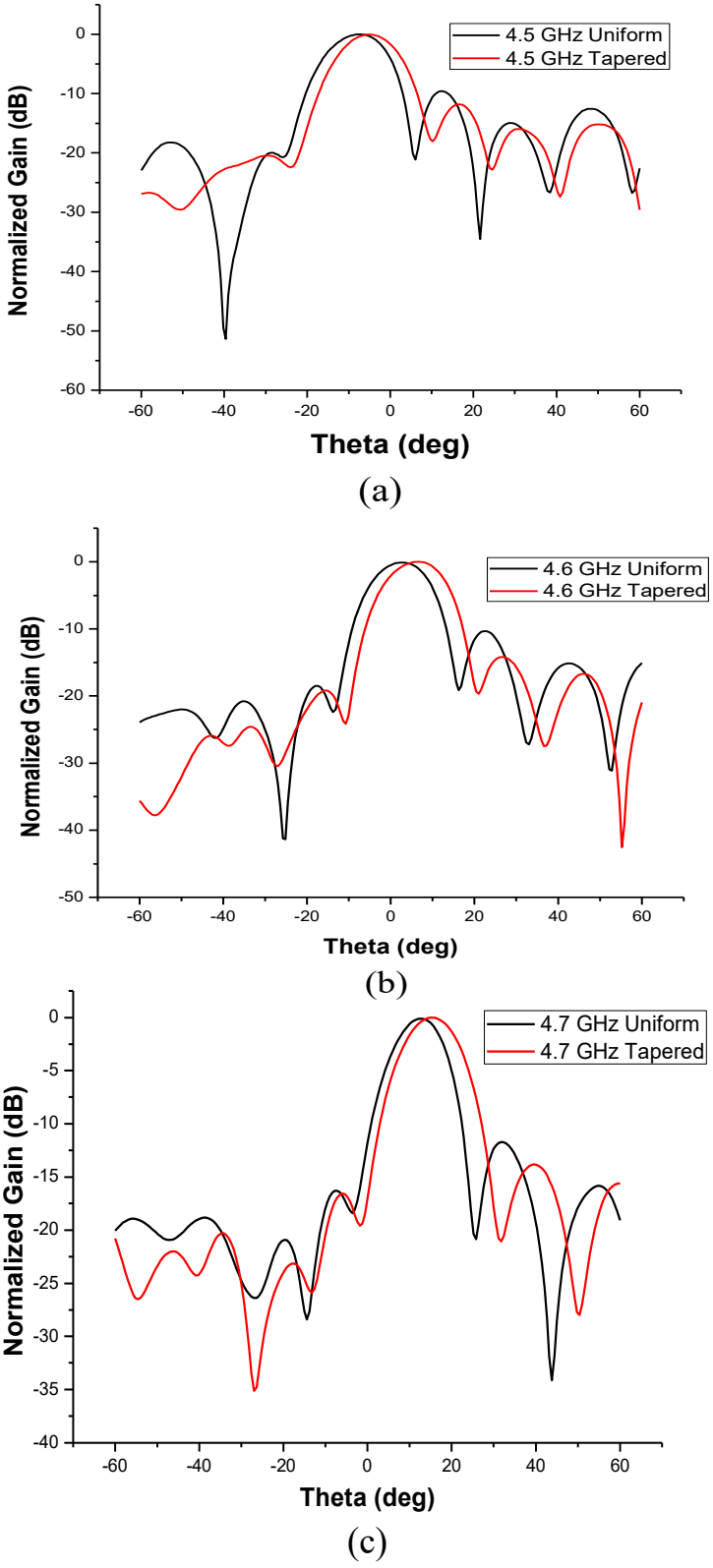

Figure 17 the normalized gain for both conventional and tapered antenna. (a) 4.5 GHz (b) 4.6 GHz (c) 4.7 GHz

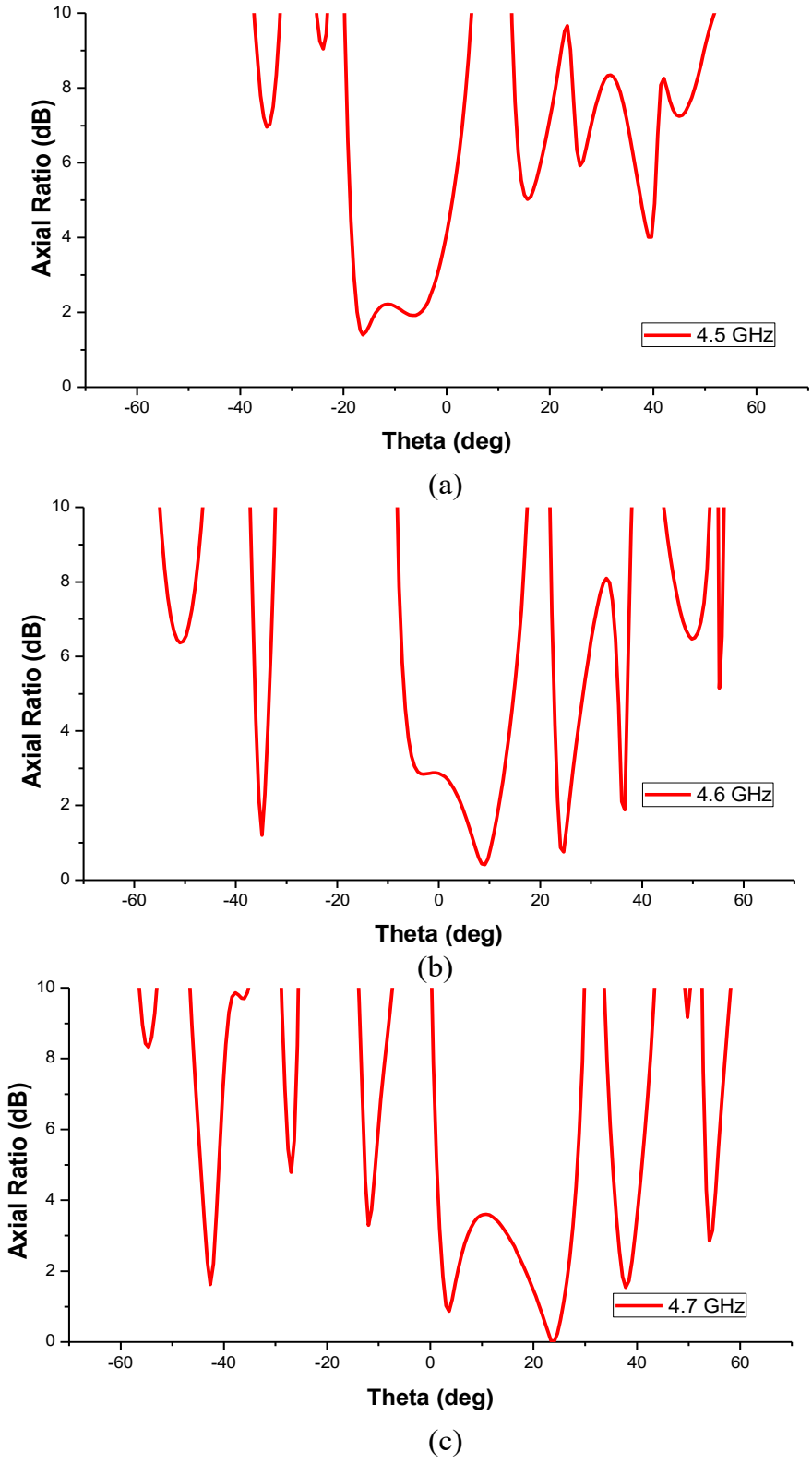

Figure 18 the axial ratio of the tapered antenna along theta. (a) 4.5 GHz (b) 4.6 GHz (c) 4.7 GHz

The axial ratio of the tapered antenna is measured to evaluate the circularly polarization (Figure 18). The graph shows that the tapered antenna has axial ratio below 3 dB in the direction where main beam exists at 4.5 GHz and 4.6 GHz. At 4.7 GHz, the axial ratio has a jump slightly above 3 dB. This is because 4.7 GHz is away from the center frequency, the phase delay deviates from 90° between the adjacent interdigital slots.

Chapter 2

Blazed Metasurface Grating and Application in Waveguide

2.1 Introduction

A metasurface (MS) is a two dimensional structure (practically of thin thickness) that can provide abrupt phase and amplitude discontinuities in the field, generally by tailoring the transmission/reflection properties of the surface [13]. Metasurfaces provide a versatile way to control the wave front and extend their classical predecessors, namely gratings [14] and frequency selective surfaces [15]. They have been demonstrated at various frequencies from microwaves all the way to optical frequencies, and are typically formed from an arrangement of sub-wavelength scatterers with electric and/or magnetic response. Thin devices for various objectives have been proposed so far using Metasurfaces, e.g. for arbitrary refraction [13, 16], flat lensing and polarization control [13], to name a few.

In this work, we intend to mimic the operation of a blazed grating using a planar metasurface, and thus create a "blazed metasurface grating". The blazed MS can reflect an oblique incident wave back in the direction of incidence, and also produces reduced specular reflection, similar to the blazed grating [14]. Strip gratings on thick grounded dielectric slab were also shown to provide strong blazing in TE and TM polarizations [17, 18]. In this project, we use phase modulation to implement the metasurface.The incident angle in this case is set to be 30° as an example. These behaviors are confirmed by simulation and scattering measurements of a fabricated sample. The blazed MS is designed to replicate equivalent surface currents of a blazed grating.

As a further demonstration, a guided wave scenario is investigated, where the blazed MS is used in a waveguide side-wall. It is shown that that it opens a high-rejection stopband in the transmission spectrum, confirming that specular reflection is highly rejected. All designs are verified with simulations and measurements. The blazed MS can find various applications, providing a flat low-profile alternative to corner reflectors, existing situations where non-planar blazed gratings are used, or in mirrors of Fabry-Perot cavity resonators, to name a few.

2.1.1 Blazed Grating

A diffraction grating is a periodic structure which can scatter an incident wave into different directions. It is usually used as the reflector for resonator which allows single frequency resonance. A blazed grating is one type of diffraction grating, and a sawtooth grating is a prime example of a blazed grating. The main characteristics of a sawtooth blazed grating is the periodicity d and blazed angle θ_b (Figure 19).

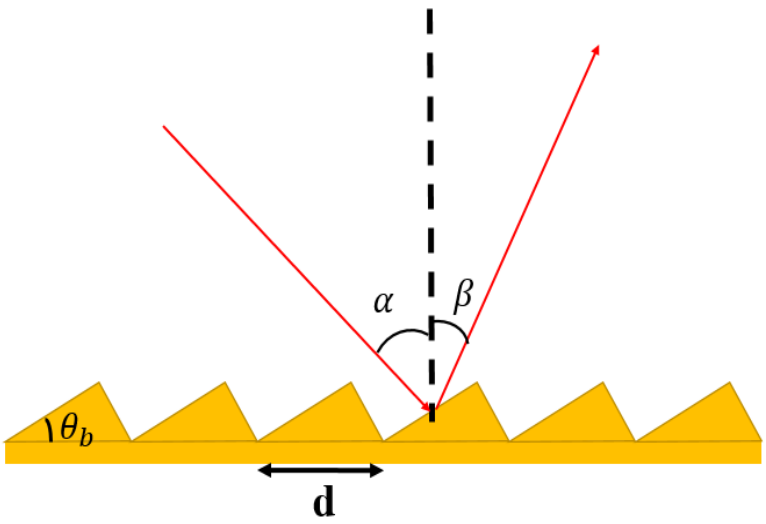

Figure 19 Scheme of the blazed grating

The different propagation modes of the scattered waves from the blazed grating are noted as grating modes. These modes are caused by the additive interference of the waves diffracted

by each unit cell. Thus, the grating modes are dictated by the frequency, incident angle α, scattered angle β and periodicity d. Since the condition for additive interference is the optic path difference for adjacent diffracted wave to be mλ, it is easy to predict the diffraction order by:

$$d(\sin(\alpha) + \sin(\beta)) = m\lambda \qquad (2.1)$$

Equation 2.1 is called grating equation where m represents the index of the diffraction order. Given any three of the four parameters (α, β, d, m), the rest can be obtained from the grating equation. The zeroth order mode indicates no diffraction, the scattered wave follows the specular reflection law as hitting a mirror. In many cases, the blazed grating is employed to maximize the m=-1 mode while minimizing the zeroth mode.

A more special case is called Littrow configuration when $\alpha = \beta = \theta_b$. In this case, the incident wave is normally incident to the oblique surface and going back into the same direction. Thus, the grating equation leads to

$$\alpha = \beta = \theta_b = \arcsin(\frac{m\lambda}{2d}) \qquad (2.2)$$

2.1.2 Phase Control Using Metasurface

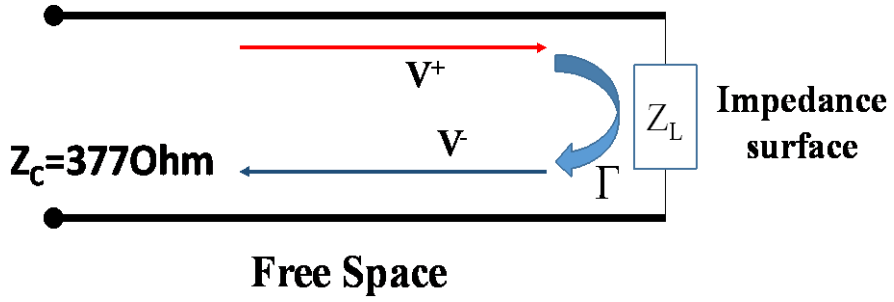

Figure 20 the circuit model of the reflection problem

The phase control is implemented by reactive impedance surface (RIS) in this case. To understand the principle, let us consider the circuit model of a subwavelength unit-cell of

periodic problem where a plane wave is normally incident on a surface and reflected (Figure 20). The free space can be seen as a transmission line whose characteristic impedance $Z_C = 377\Omega$. The surface which reflects the wave can be seen as a termination with a certain impedance Z_L. The incident and reflected wave are noted as V^+ and V^- correspondingly. From the transmission line theory, the reflection coefficient is

$$\Gamma = \frac{Z_L - Z_C}{Z_L + Z_C} \tag{2.3}$$

The relationship between incident and reflected wave is

$$V^- = \Gamma V^+ \tag{2.4}$$

If Γ is real number, then the reflected wave and incident wave will only have magnitude difference and no phase difference. However, if the impedance of the surface is reactive i.e. the impedance is complex number, the Γ will be complex whose phasor form is Ae^{ϕ}. In this case, the reflected wave will have phase difference ϕ with the incident wave. In consequence, the phase of the reflected wave can be controlled by controlling the reactive impedance of the surface.

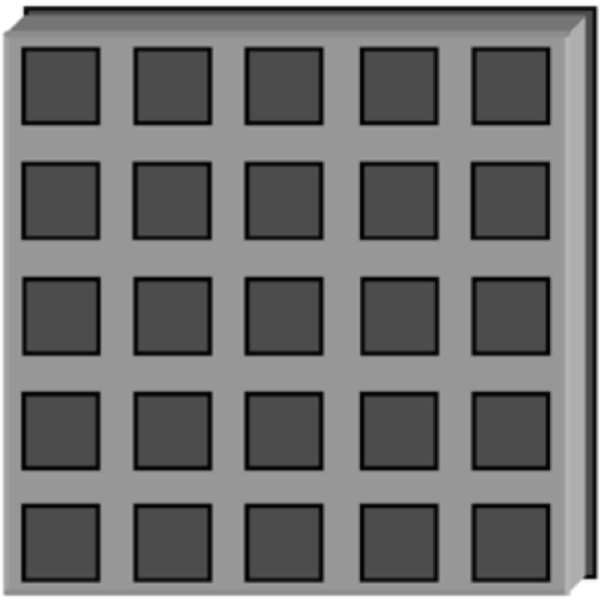

Figure 21 a normal design of RIS

A normal RIS is shown in Figure 21 [19]. It is a PCB whose one side is periodic square patches while the other side is metal ground.

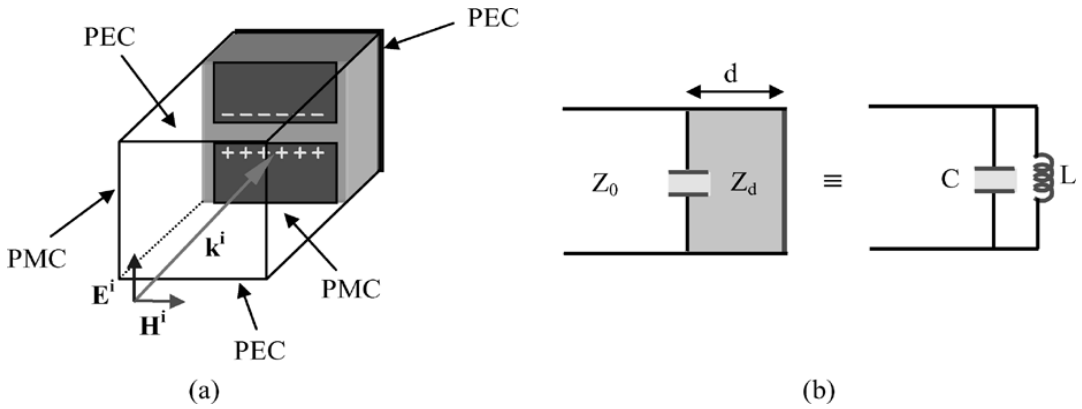

Figure 22 the investigation for unit cell. (a) the unit cell structure (b) the equivalent circuit model

The circuit model of a unit cell is given in Figure 22 [19]. A PEC-PMC waveguide is made to support plane wave to propagate. The electric field across the gap causes the electric charge to build up along the edge of the patches which will make the gap a capacitor. On the other hand, from the transmission line theory, the input impedance of the short terminated transmission line is given by:

$$Z_{in} = jZ_0 \tan(\beta d) \qquad (2.5)$$

When d is smaller than quarter wave length, the reactive input impedance is positive which indicates an inductive input impedance. Thus, a parallel LC circuit is proposed to be the equivalent circuit as shown in Figure 22 (b). The shunt LC circuit is open (PMC) at resonance, inductive below resonance frequency and capacitive above resonance frequency. A comparison between FDTD simulation and circuit model is presented in Figure 23, which shows the phase difference behaves as we expected. For oblique incident, the principle is same and the results holds [19]. Thus, the phase difference between incident and reflected wave can be controlled by tuning the resonance frequency.

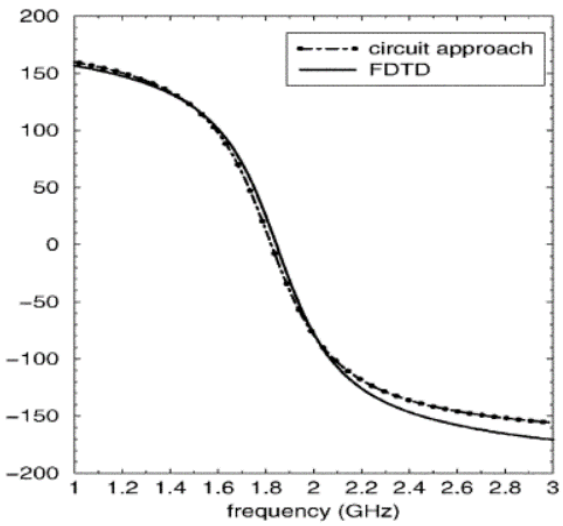

Figure 23 the phase difference of the proposed RIS

2.2 Design Guideline

In this work, a metasurface which mimics blazed grating with Littrow configuration is proposed. The goal for this grating is to minimize the zeroth mode (specular reflection) and maximize the -1 mode. The center frequency of the structure is set to be 10 GHz and incident

angle is 30°.

2.2.1 Design for the Phase Distribution

Given the objective of the project, the 3D blazed grating can be easily designed. At 10 GHz, the free space wavelength is $\lambda_0 = 3\text{cm}$. Considering the Littrow configuration, the blazed, incident and -1 mode angle all equal to 30°. Thus, the periodicity of the blazed grating can be easily calculated through the reduced grating equation (2.2). In this case, periodicity $d = \lambda_0 = 3cm$. The aforementioned sawtooth blazed grating depicted in Figure 24 (a), reflecting the waves mainly back in the path of incidence. This is contrary to the completely specular reflection from a solid perfect conductor. The period dictates the angles of diffraction for a certain incidence, whereas the blaze angle (θ_b) in Figure 24 (a) mainly determines the amount of power in the diffracted orders.

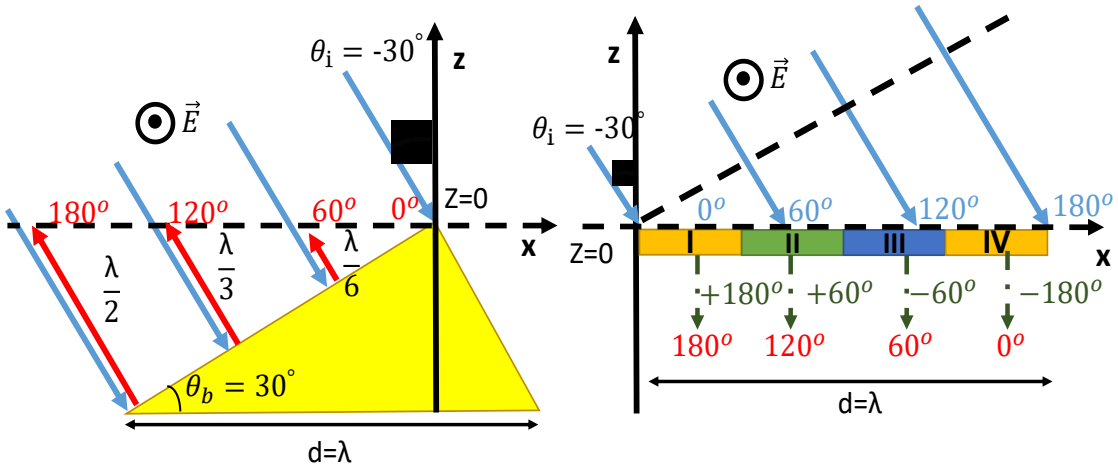

Figure 24 (a) Unit-cell of a blazed grating (periodic in *x*) reflecting an incident wave θ_i = -30° back in the direction of θ_{-1}= -30°. (b) Unit-cell of an equivalent blazing metasurface (periodic in *x*) reflecting waves in a similar manner, realized with four reflection phase regions

A metasurface is proposed in Figure 24 (b) to mimic the blazed grating in Figure 24(a). The ray optics method is employed to implement the phase distribution. As shown in Figure 24 (a), the phase of the reflected wave at z=0 along x axis is calculated. This phase distribution

is c the optic path length. While the 180° phase change due to PEC boundary condition is cancel out because the phase distribution is relative with each other. As shown in Figure 24 (a), at z=0, this scattered field has a constant amplitude with a linear phase variation over x. We can replace the non-planar blazed structure with an equivalent planar metasurface placed at z=0, as long as the MS can provide tangential surface currents that create the same scattered field, under the oblique plane-wave incidence [20]. Here, a polarization of TE, i.e. the electric field is transverse to the plane of incidence, is considered. Same principle also holds for the TM incident. As shown in Figure 24(b), the MS is sectioned into 4 sections for design simplicity and robustness against tolerances. When the wave incident on the MS, the phase variation is linear because of the optics path difference. To achieve the same phase variation as the 3D blazed grating, a certain phase change is needed and shown in Figure 24(b).

2.2.2 Implementation of the Metasurface

From the previous section, the phase changes needed in each region on MS have already been described. We need to design the aforementioned reactive impedance surface to implement the phase difference. In this case, the substrate is Rogers RT/duroid® 6010LM with dielectric constant ε_r=10.2 at 10GHz and thickness H=1.9mm, and backed by a copper conductor.

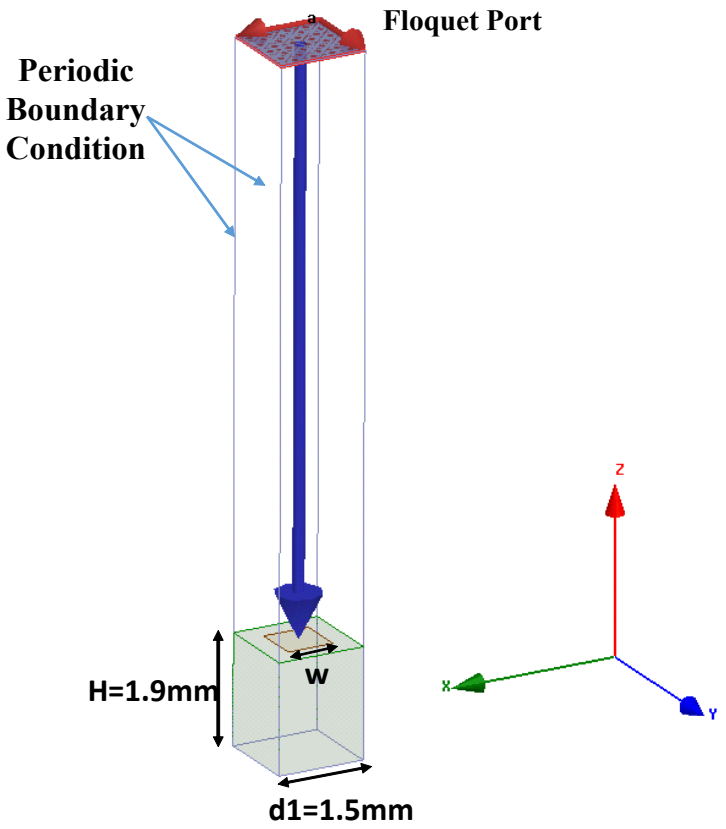

Figure 25 the simulation for single patch. Electric field is in y direction (TE), the incident angle is 30°. Floquet port is deembed to the surface of the patch

The unit cell is shown in Figure 25. The period of the unit cell is 1.5mm, and is thus very subwavelength such that only specular reflection exists. The side walls use the periodic boundary condition with proper phase delay such that a 30° incident angle in x-z plane is implemented. The top wall is a Floquet port which is deembeded to the surface of the patch for convenience. The electric field is in the y-direction (TE). The square patch has dimension w which will be tuned for desired phase change. Since the Floquet port is deembed to the patch, the phase change can be simply found by checking the angle of S_{11}. The relationship between phase difference and patch dimension is obtained by a parametric sweep on w in HFSS. The result is shown in Figure 26.

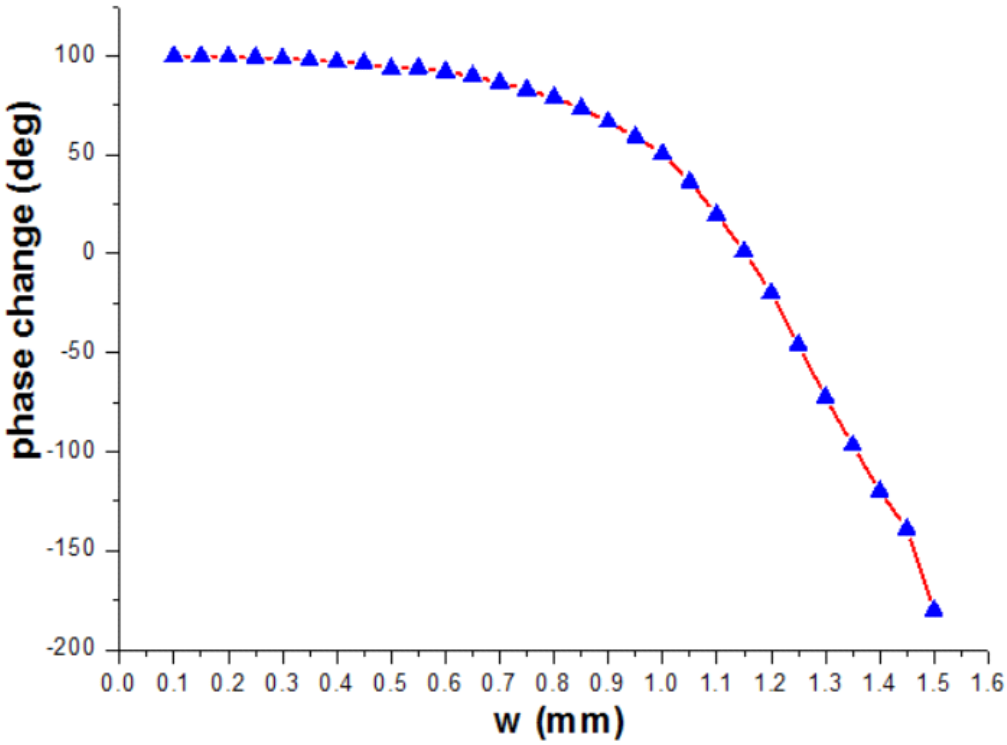

Figure 26 the relationship between patch dimension and phase change. The w starts from 0.1mm to 1.45mm with 0.05mm step

It can be seen that the phase difference between incident and scattered wave starts from 100º and decrease as the patch dimension w increases. That indicates a phase advance when w is small and phase delay when w is large. Another observation is that a phase +180° is not possible with this chosen substrate and shape. The upper limit of the phase change is 100° because of the optical path in inside the substrate. On the other hand, the lower limit can achieve -180 when the patch covers the whole unit cell, i.e. PEC boundary condition. However, the -180 and +180° phase change are equivalent because they are same when unwrapped. In addition, the phase becomes very sensitive when w is large. Even small error in w can cause huge phase error.

From Figure 26, the desired phase change can be obtained by using proper patch dimension. The combinations are listed in Table 2.

Table 2 the patch dimension for corresponding desired phase change

Region on the MS	Desired Phase Change (deg)	Patch Dimension (mm)
I	+180	1.5
II	+60	0.95
III	-60	1.27
IV	-180	1.5

Using the dimensions given in Table 2, the metasurface can be implemented (Figure 27). For convenience of simulation and measurement, the design has only 4 units. Thus, the total dimension of this MS is 12cm by 12cm.

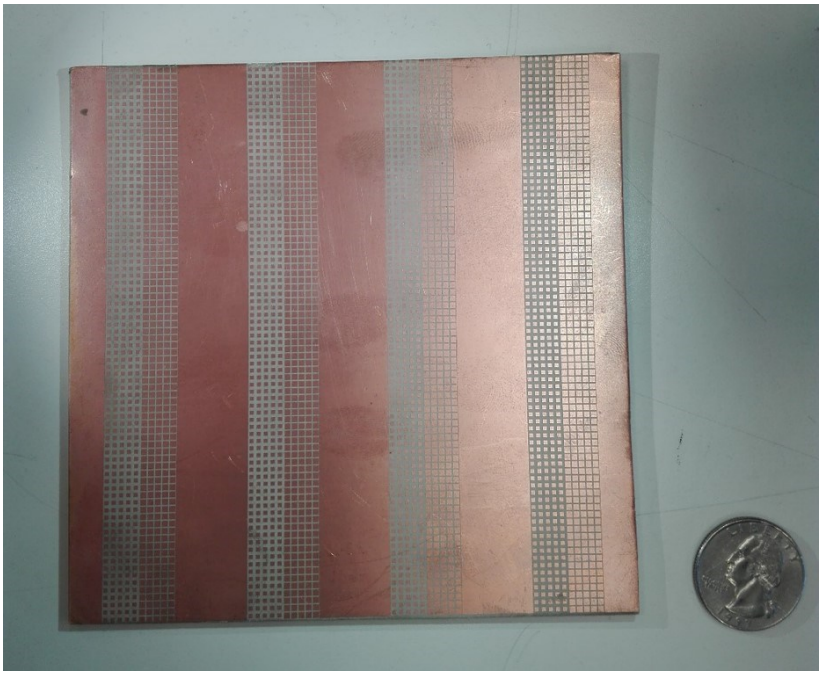

Figure 27 Metasurface with only four units

2.2.3 Strip Type Metasurface

In previous section, a MS using small patches is proposed. It should be noted that the gaps between the patches provide capacitance thus forming the reactive impedance surface. For TE incident wave (E in y direction), only the gaps perpendicular to E field will behave as capacitors.

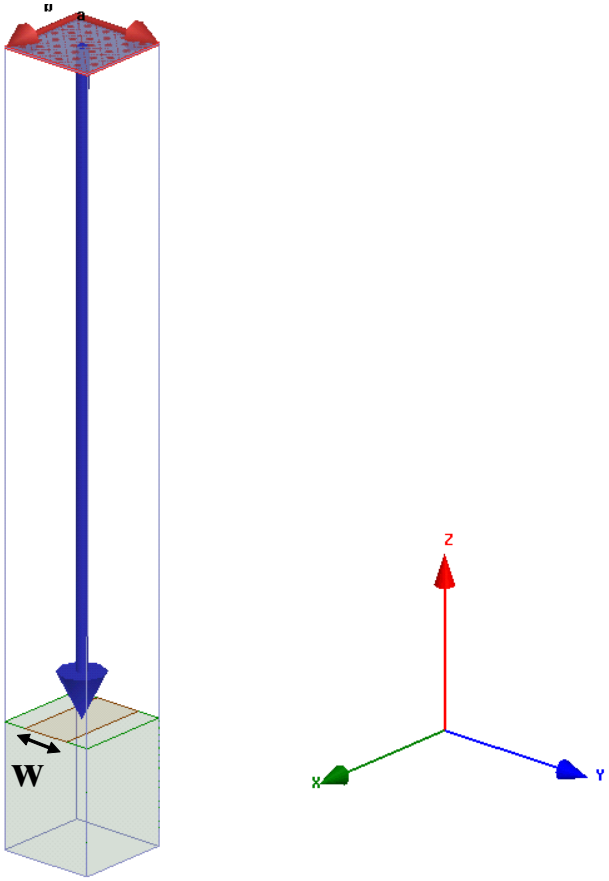

Figure 28 Unit cell for strip type RIS. The patch extends to strip such that only gaps perpendicular to E field is preserved

Since the gap parallel to E field is not important in this case, the patches can be connected with each other along x direction. Thus, only the gaps in x direction are preserved. However, for TM

incident wave (H field in y direction), the E field cannot see any gap. In this case, the metasurface should behave as a PEC. This would tremendously reduce the difficulty in simulation and fabrication. The unit cell simulation is the same as the previous except that the patch extends to a strip which touch the periodic boundary in x direction (Figure 28).

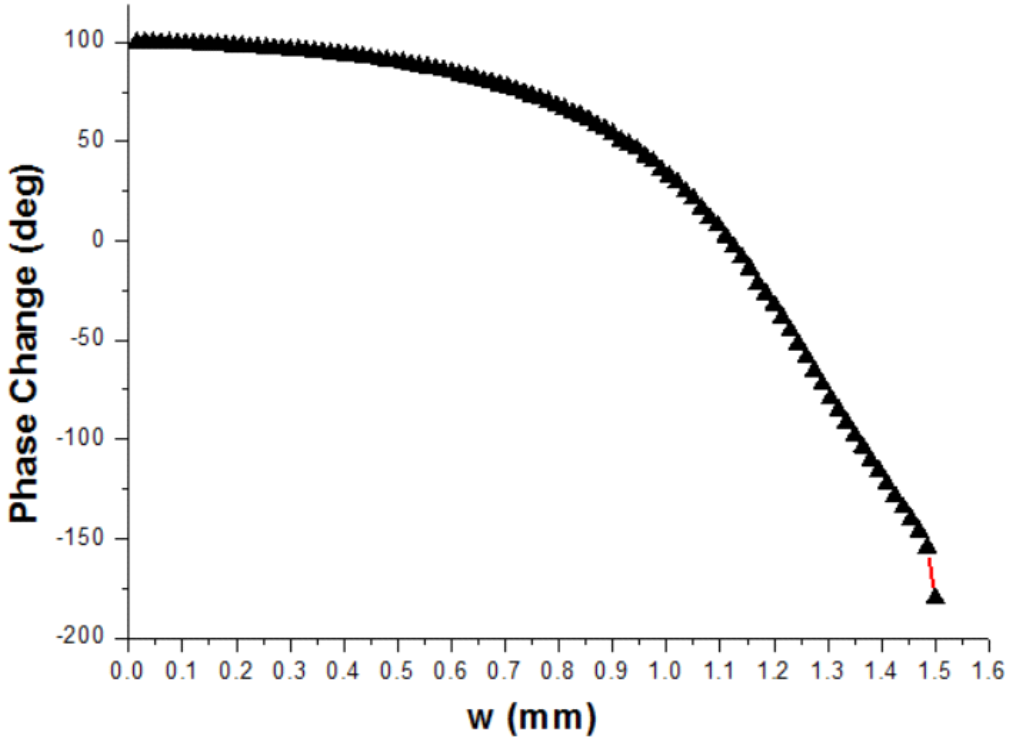

Figure 29 the relationship between the strip width and phase change. The w starts from 0.015mm to 1.5mm with 0.015mm step

Similar to previous section, the relationship between the strip width w and phase change is obtained through parametric sweep (Figure 29).

The “phase change – strip width” relationship shows the same characteristics as the patch case. This fits the expectation we made since they follow same principle. Thus, the design

parameters are given from Figure 29 and showed in Table 3.

Table 3 the strip width for corresponding desired phase change

Region on the MS	Desired Phase Change /deg	Strip Width/mm
I	+180	1.5
II	+60	0.74
III	-60	1.17
IV	-180	1.5

Using the data in Table 3, a similar metasurface is designed (Figure 30). The dimension for this MS is also 12cm by 12 cm.

2.3 Measurement

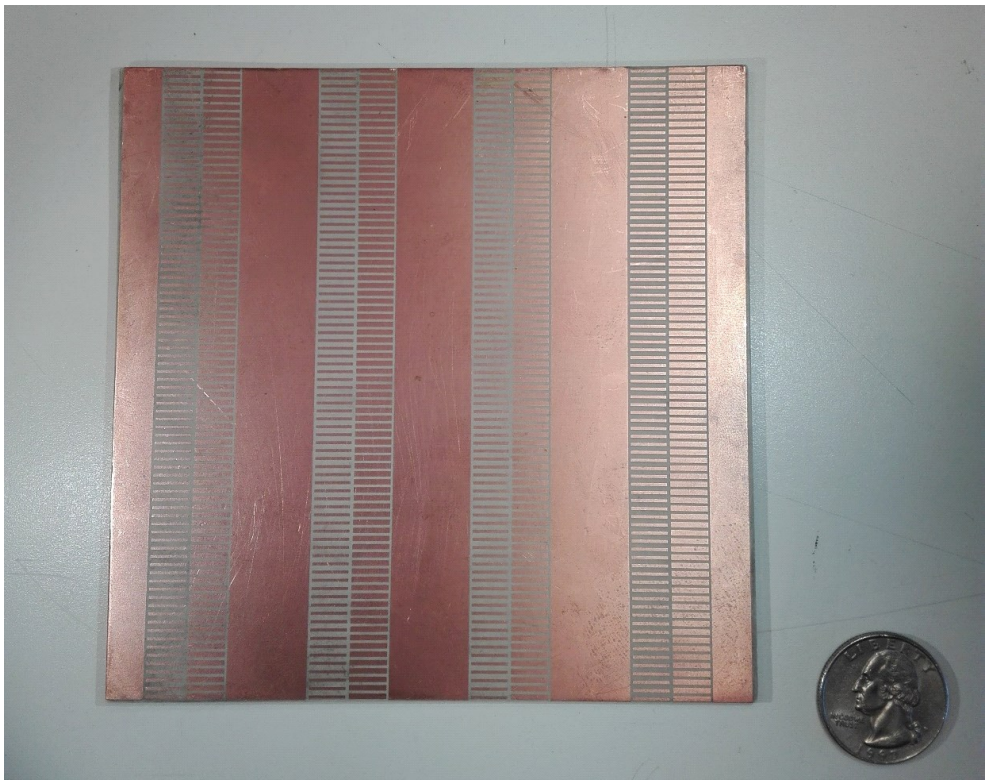

Figure 30 Strip type metasurface with 4 units

To measure the effect of the MS, we need to measure the scattered field pattern in x-z plane. Here, we choose to measure bistatic radar cross section (RCS) to better quantify the result and

compare with the simulation.

2.3.1 Measurement Setup

Due to the limit of the equipment, the RCS measurement is conducted on the roof which is an open space. To further reduce the noise, absorbers are also used. The measurement set up is shown in Figure 31.

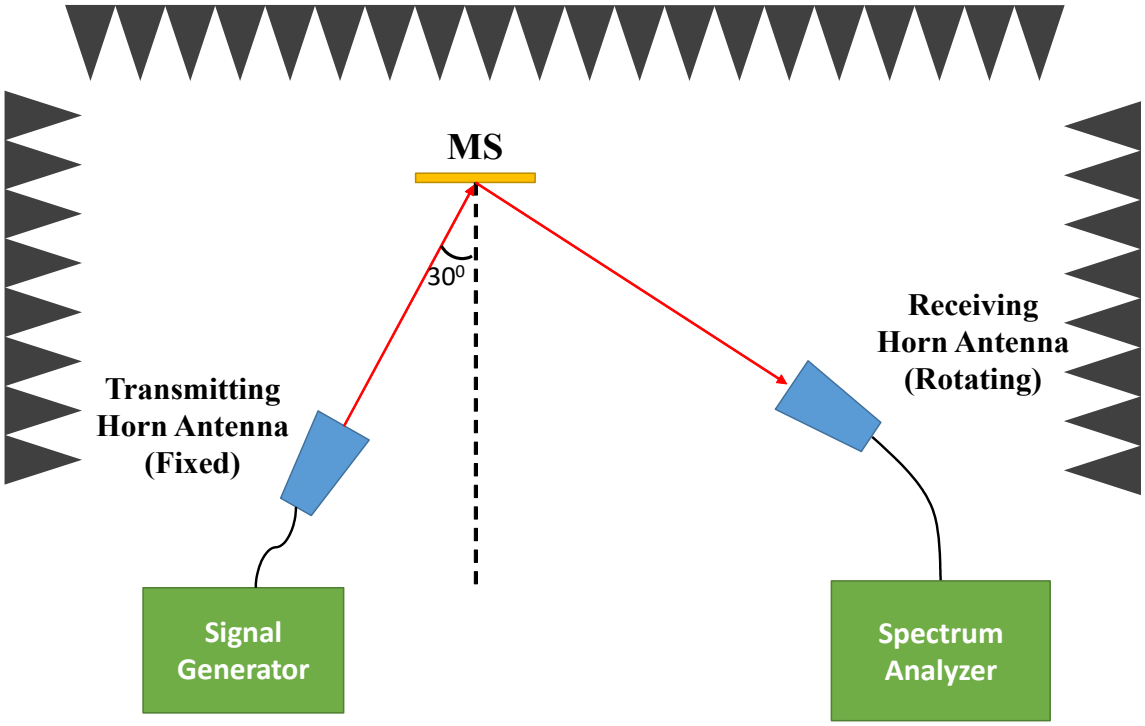

Figure 31 the measurement set up (a) real measurement setup (b) the scheme of the measurement setup

As can be seen in Figure 31, two horn antennas are used in the measurement. The one which is connected to signal generator is the transmitting antenna. It is fixed such that the beam is incident on the MS with a 30° incident angle. The other horn antenna is connected to

spectrum analyzer and behaves as receiving antenna. The receiving antenna can rotate around the MS to measure the scattered field at different angles thus collecting the bistatic RCS. For measuring RCS, a 12cm by 12cm metal plate is measured. The result are normalized to the analytical result and become the benchmark for the MS measurement results. To compare the MS with 3D blazed grating, a 12cm by 12 cm sawtooth grating is also fabricated and measured for comparison (Figure 32). It is made with card paper and covered with copper tape.

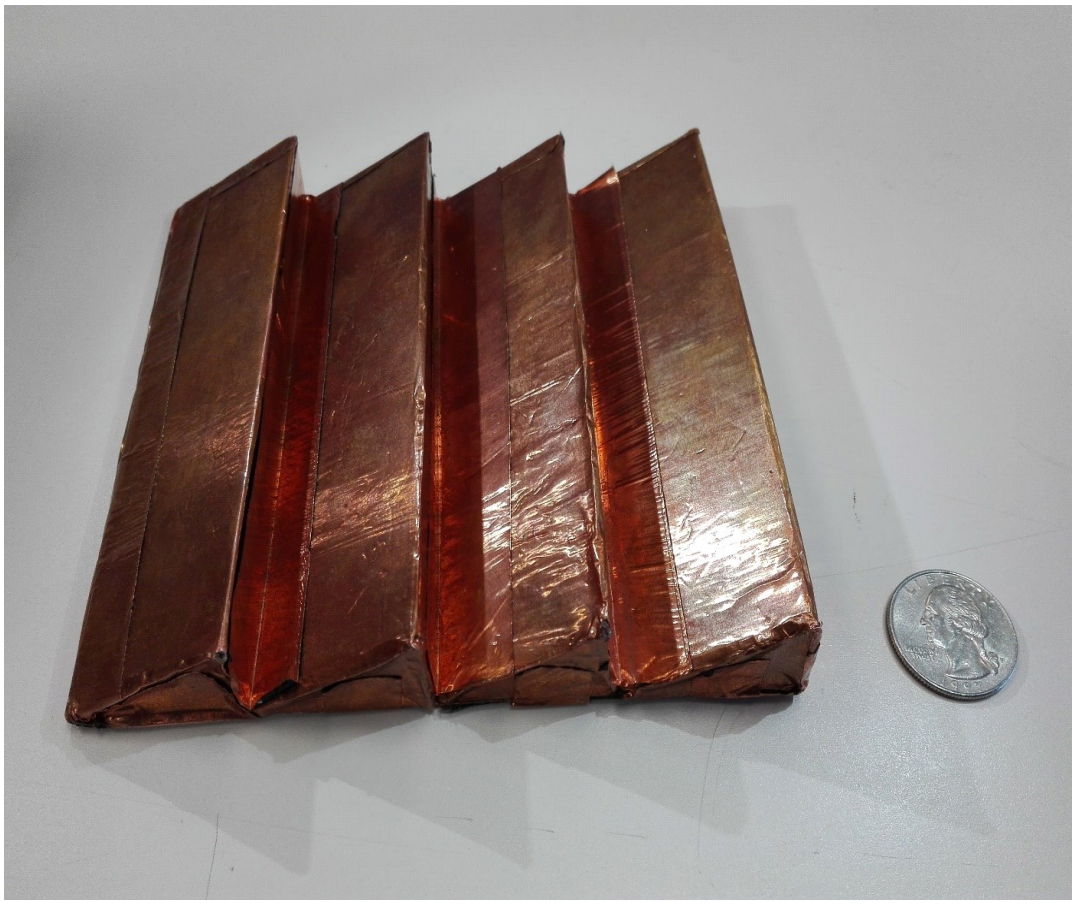

Figure 32 the fabricated sample of 3D blaze grating

For the evaluation and reference for later measurement, the RCS of the 3D blazed grating and metal plate is conducted. The result is shown in Figure 33.

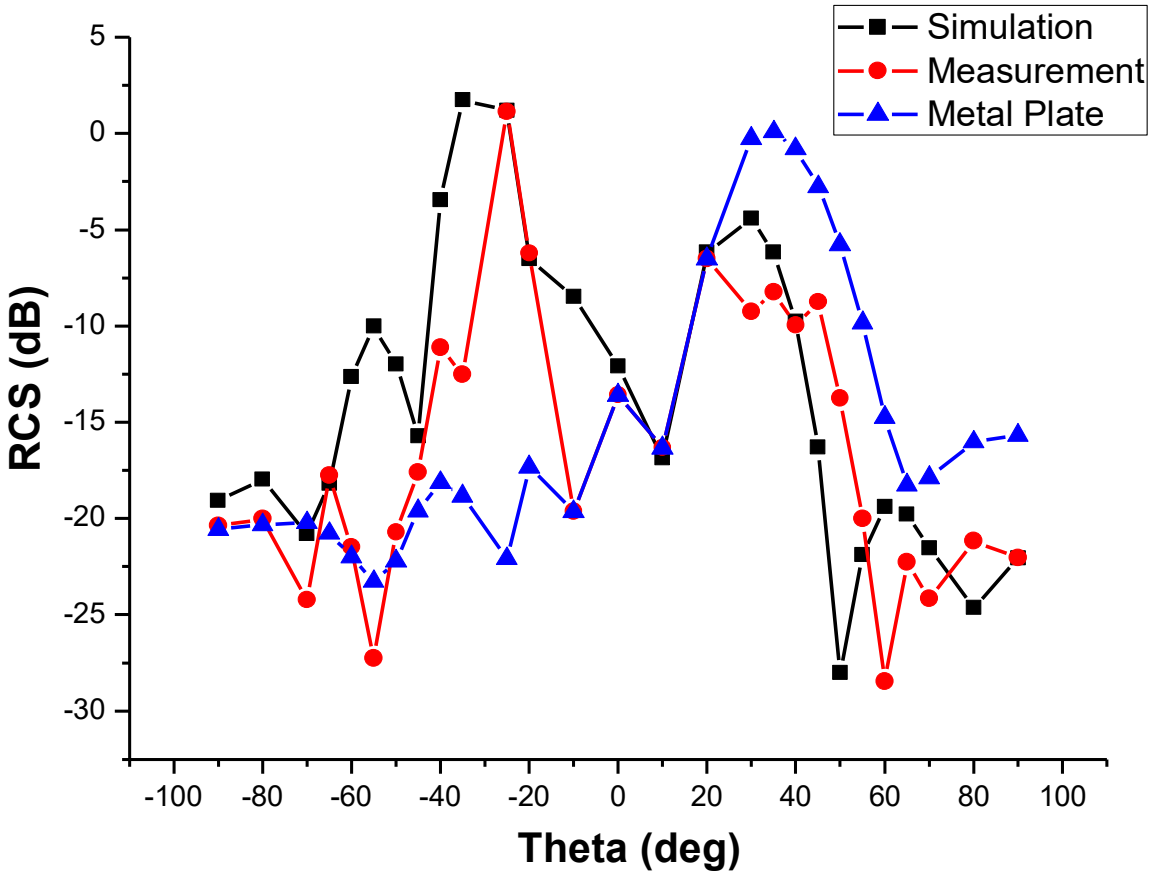

Figure 33 the simulation and measurement result for 3D blazed grating and Metal Plate

Since the transmitting antenna is located at $\theta = -30^0$, the specular reflection should be at $\theta = 30^0$ according to Snell's law. Meanwhile, the m=-1 mode should locate at $\theta = -30^0$ according to grating equation under Littrow configuration. In Figure 33, a strong scattered field is shown at $\theta = 30^0$ for metal plate. This the specular reflection. For all other directions, the scattered field is small. For the 3D blazed grating, a strong field appears when $\theta = -30^0$. This is the -1 mode which is desired. On the other hand, the specular reflection for 3D blazed grating is shown to be reduce by around 5dB compared with the metal plate. In addition, the measurement result agrees with the simulation well.

2.3.2 Measurement Result for Small Patch MS

The measurement result for small patch MS is shown in Figure 34. The RCS of small patch

MS is very similar with 3D blazed grating. The strong -1 mode can be observed at $\theta = -30^0$ while the specular reflection is greatly reduced. Compared with the 3D grating, the -1 mode is slightly lower by around 2dB. Consequently, the specular reflection of small patch MS is slightly higher than 3D grating by around 2dB. The simulation result is slightly better than measurement result. The difference comes from the fabrication errors and the measurement errors.

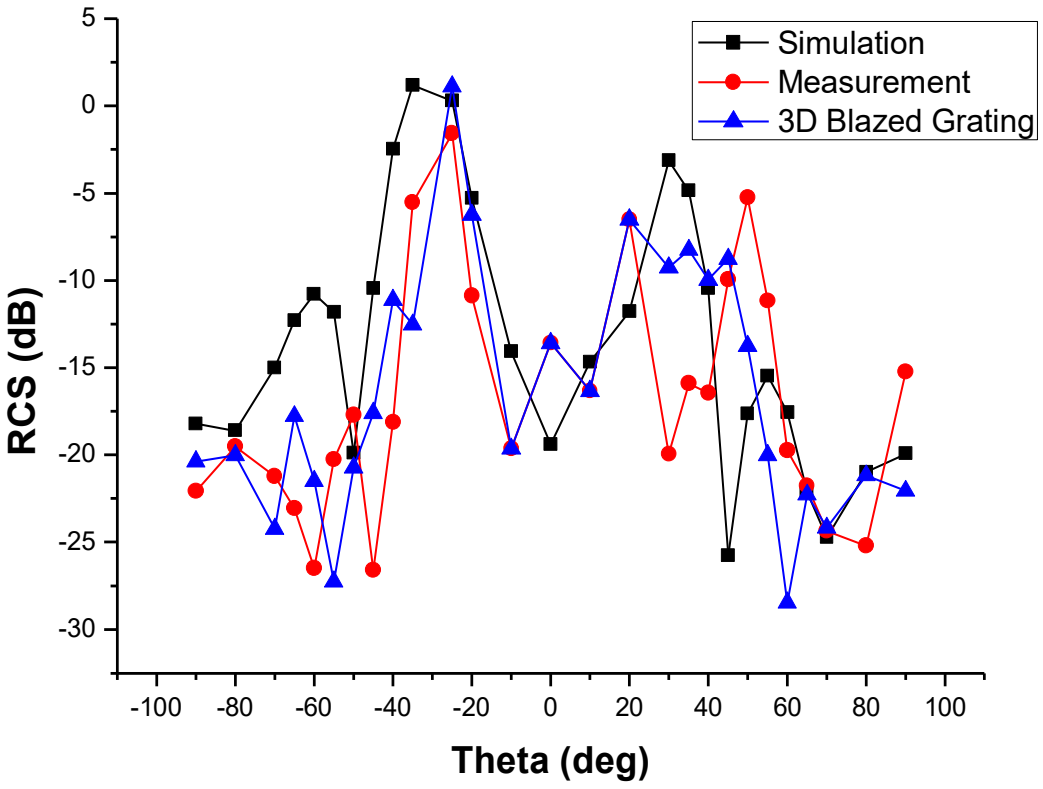

Figure 34 the simulation and measurement result for small patch MS

2.3.3 Measurement Result for Strip MS

The measurement result of the strip type MS is presented in Figure 35. From the graph it can be observed that the strip type MS has almost the same response as the 3D blazed grating. Both of them show a strong -1 mode and small specular reflection.

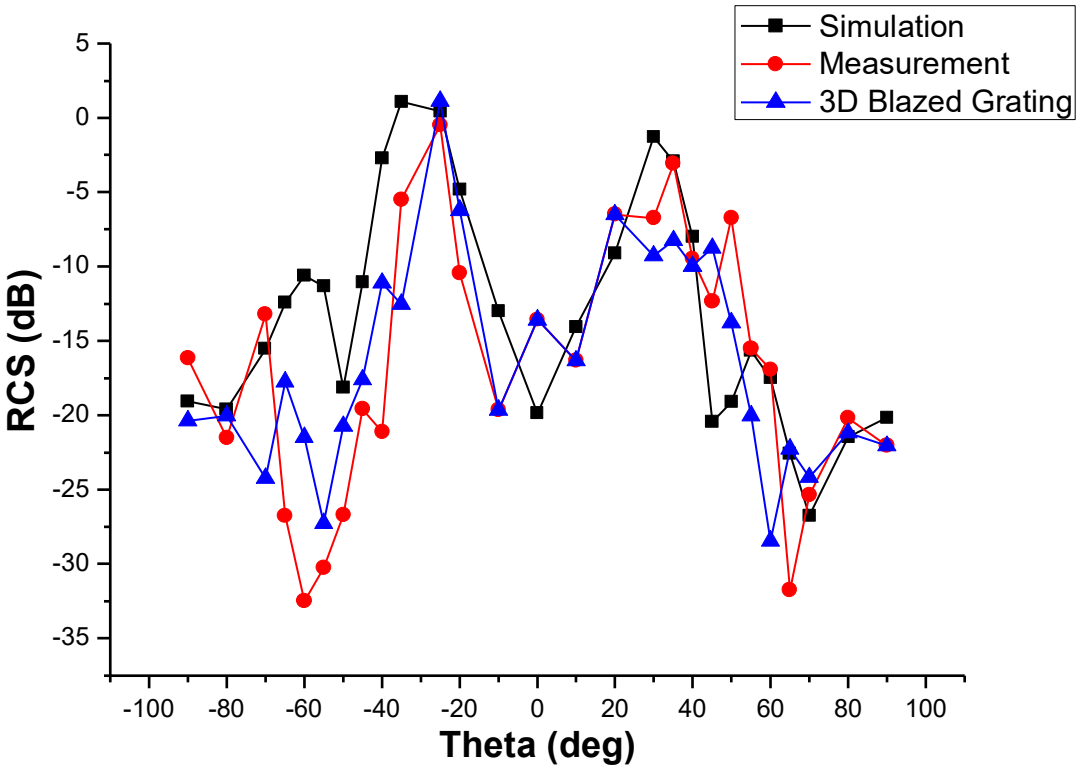

Figure 35 the simulation and measurement result for strip MS

2.4 Application of the MS in Waveguide

We investigate the response of a waveguide operating in the TE_{10} mode in the X-band, when one sidewall of the guide is replaced with the blazed metasurface. In this application, the strip type MS is used. The scenario is shown in Figure 36. The electric field of the TE_{10} points in the y-direction, which is the polarization suitable for the operation of the MS, given its orientation within the waveguide.

The motivation for this experiment is to utilize the specular rejection of the blazed metasurface, in a guided wave scenario. The TE_{10} mode established inside a waveguide with PEC walls can be written as the sum of two oblique plane waves [21], reflected specularly with respect to each other. By lining one sidewall of the guide with the blazed MS, we expect to minimize the specular reflection on the sidewall and thus avoid establishing the TE_{10} mode in

the guide, for the range of frequencies where the MS operates well.

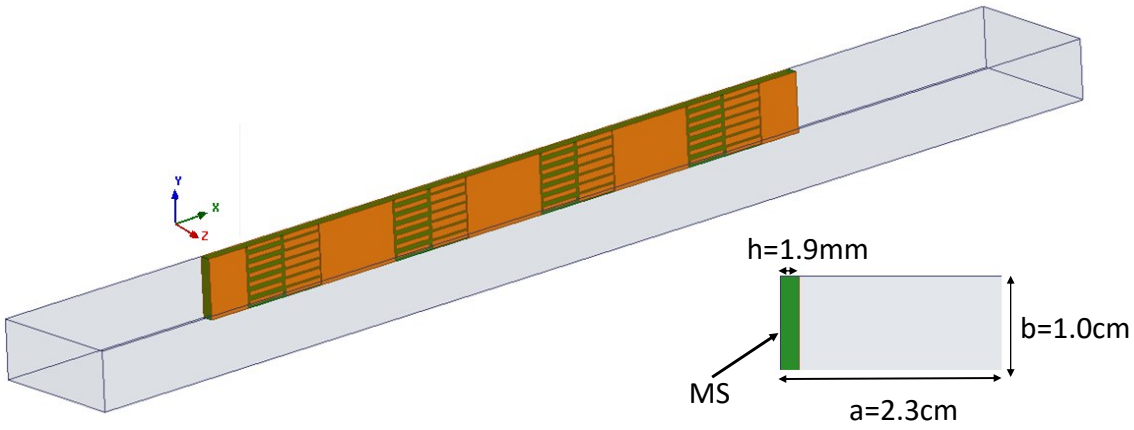

Figure 36 An air filled X-band waveguide lined with a 4-cell blazed metasurface on one sidewall.

The S-parameter measurements of the waveguide lined with a 4-cell metasurface is shown in Figure 37. It can clearly be seen that a stopband with high rejection opens up in the spectrum from 10.6 to 12.4 GHz. The start of the bandstop is slightly above the design frequency at which specular reflection reduces, which is mainly due to fabrication inaccuracies of the prototype. The frequency with the highest stopband rejection level is observed around 11.2GHz. This frequency is in fact the frequency where the MS was found to have the highest specular reflection rejection, irrespective of the incident angle.

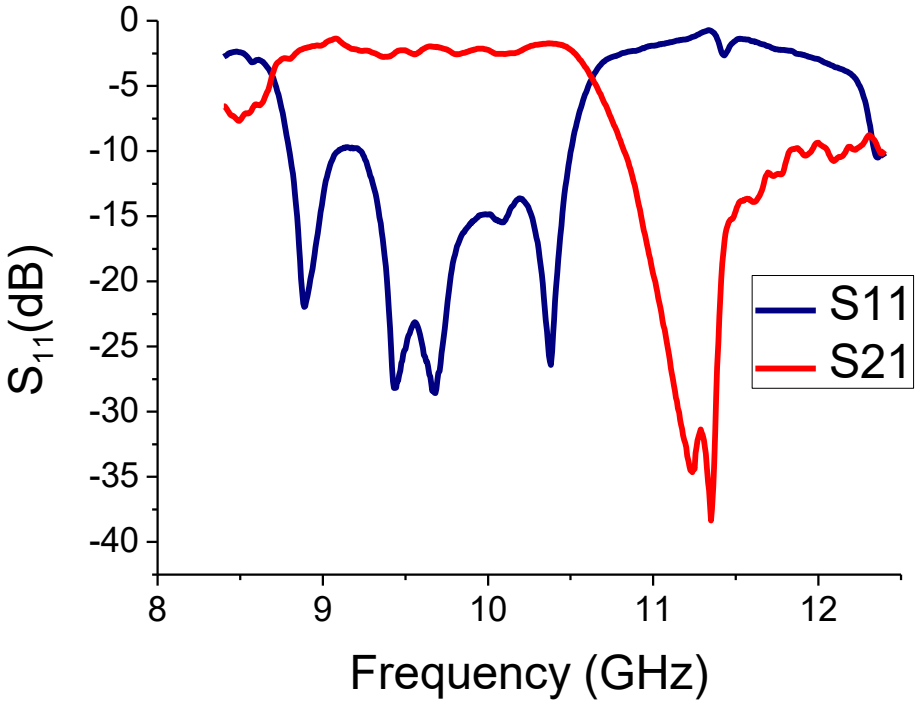

Figure 37 S-parameters of the waveguide lined with blazed metasurface.

It should be noted that by inserting the MS into the waveguide, we have effectively reduced the long dimension of the waveguide cross-section. However, a PEC waveguide of these reduced dimensions still has a TE_{10} mode cutoff of 8.6 GHz. This can be seen in the response, showing transmission from 8.6 GHz to 10GHz. The MS does not reject specular reflection below 10GHz, and acts more like a PEC wall, or more precisely, as an impedance sheet.

CONCLUSION

The Circularly Polarized Low Side Lobe Level Composite Right/Left-Handed SIW Leaky Wave Antenna is proposed in this work. To this end, the CRLH transmission line theory and the concept of leaky wave antenna are initially reviewed, followed by the proposed design. The circularly polarization is achieved by the orthogonal pairs of interdigital slots with 90°phase difference. On the other hand, low side lobe level is achieved by tapering the leakage amount of each unit cell. To control the leakage amount, the topology of the slots of each cell are specifically designed such that the dispersion diagram satisfies the condition where the two adjacent slots have 90°phase change. The design formula has been obtained within a reasonable range. The measurement of the proposed antenna demonstrates a 3 dB lower side lobe level compared with conventional CP CRLH SIW LWA. The measurement also showed good CP properties.

A planar metasurface which can mimic the operation of a sawtooth blazed grating is also proposed in this thesis. The blazed grating and the grating equation are introduced. Then the idea of using a planar structure to replace the triangular shape unit cell of a sawtooth grating is presented using ray optics approach. The planar structure is designed such that the incident wave can be backscattered by imposing a certain phase change to provide proper phase of scattered field along the surface. The phase change is implemented with reactive impedance surface. Two type of impedance surface are designed for a blazed grating auto-collimation at 10 GHz for 30° incident. The design can discriminate the polarization of the incident wave. The bistatic RCS measurement is performed on both of the designs. The result shows a good

rejection for specular reflection and strong m=-1 mode (backscatter). The planar designs in this thesis provide flat low-profile solutions for leaky-wave and blazing operations.

REFERENCE

[1] L. Liu, C. Caloz, and T. Itoh, "Dominant mode (DM) leaky-wave antenna with backfire-to-endfire scanning capability", Electron. Lett., vol. 38, no. 23, pp.1414 -1416, Nov. 2002.

[2] Tavallaee, Amir A., et al. "Active terahertz quantum-cascade composite right/left-handed metamaterial." Appl. Phys. Lett 102.2 (2013).

[3] Lim, Sungjoon, Christophe Caloz, and Tatsuo Itoh. "Metamaterial-based electronically controlled transmission-line structure as a novel leaky-wave antenna with tunable radiation angle and beamwidth." Microwave Theory and Techniques, IEEE Transactions on 53.1 (2005): 161-173.

[4] Y. Dong and T. Itoh, “Composite right/left-handed substrate integrated waveguide and half mode substrate integrated waveguide leaky-wave structures,” IEEE Tran. Antenna Propagation, vol. 59, no. 3, pp. 767-775, Mar. 2011.

[5] Hanseung Lee, Yoshiaki Kasahara, and Tatsuo Itoh, "Study of high efficiency and low sidelobe level CRLH leaky-wave antenna based on short-termination and tapered cells," 2014 European Microwave Conference, Oct. 2014.

[6] Pozar, David M. Microwave engineering. John Wiley & Sons, 2009.

[7] Caloz, Christophe, and Tatsuo Itoh. Electromagnetic metamaterials: transmission line theory and microwave applications. John Wiley & Sons, 2005.

[8] Lai, Anthony, Tatsuo Itoh, and Christope Caloz. "Composite right/left-handed transmission line metamaterials." Microwave Magazine, IEEE 5.3 (2004): 34-50.

[9] Li, Xiaoqiang, Hanseung Lee, and Tatsuo Itoh. "Studies of realizing low side lobe levels of

composite right/left-handed SIW leaky-wave antennas." 2015 Asia-Pacific Microwave Conference (APMC). Vol. 1. IEEE, 2015.

[10] Bozzi, Maurizio, Anthimos Georgiadis, and Kaijie Wu. "Review of substrate-integrated waveguide circuits and antennas." Microwaves, Antennas & Propagation, IET 5.8 (2011): 909-920.

[11] Dong, Yuandan, and Tatsuo Itoh. "Composite right/left-handed substrate integrated waveguide and half mode substrate integrated waveguide leaky-wave structures." Antennas and Propagation, IEEE Transactions on 59.3 (2011): 767-775.

[12] Lee, Hanseung, et al. "A circularly polarized single radiator leaky-wave antenna based on CRLH-inspired substrate integrated waveguide." Microwave Symposium (IMS), 2014 IEEE MTT-S International. IEEE, 2014.

[13] N. Yu and & F. Capasso, "Flat optics with designer metasurfaces," Nature materials, vol. 13, pp. 139-150, Jan. 2014.

[14] T. Itoh and R. Mittra, "An analytical study of the echelette grating with application to open resonators," Microwave Theo. Tech., IEEE Trans., vol. 17, pp. 319-327, Jun. 1969.

[15] B. A. Munk, Frequency selective surfaces theory and design, John Wiley & Sons, 2000.

[16] C. Pfeiffer and A. Grbic, "Metamaterial Huygens' surfaces: tailoring wave fronts with reflectionless sheets," Phys. Rev. Lett., vol. 110, p. 197401, 2013.

[17] Jose, K. A., and K. G. Nair. "Reflector-backed perfectly blazed strip gratings simulate corrugated reflector effects." Electronics Letters 23 (1987): 86.

[18] Cho, Y. K., U. H. Cho, and J. H. Ko. "TM‐polarized electromagnetic scattering from a

periodic strip array on a grounded dielectric." Microwave and Optical Technology Letters 11.1 (1996): 41-45.

[19] Mosallaei, Hossein, and Kamal Sarabandi. "Antenna miniaturization and bandwidth enhancement using a reactive impedance substrate." Antennas and Propagation, IEEE Transactions on 52.9 (2004): 2403-2414.

[20] Xiaoqiang Li, M. Mohammad, K. Dwaj, T. Itoh, Blazed Metasurface: The Planar Equivalent of a Sawtooth Grating, 2016 International Microwave Symposium (IMS)

[21] C. A. Balanis, Advanced engineering electromagnetics, John Wiley & Sons, 2012.